

Review

Layered Double Hydroxide-Based Photocatalysts for the Removal of Emerging Contaminants: Progress in Past Ten Years

Lingfeng Luo [†], Chen Hou [†], Lan Wang ^{*†}, Wei Zhang , Cong Wang, Junjie Liu, Yiqian Wu and Chuanyi Wang ^{*†}

School of Environmental Science and Engineering, Shaanxi University of Science and Technology, Xi'an 710000, China; lfluo0224@126.com (L.L.); hc13474605319@163.com (C.H.); zhangwei149817@163.com (W.Z.); 16683073116@163.com (C.W.); joven336@163.com (J.L.); yiqianw517@163.com (Y.W.)

* Correspondence: wanglan@sust.edu.cn (L.W.); wangchuanyi@sust.edu.cn (C.W.)

[†] These authors contributed equally to this work.

Abstract: Currently, public health is seriously threatened by the massive concentrations of emerging contaminants. Treating emerging contaminants in water using effective methods has become a major challenge worldwide. Photocatalytic technology, as an eco-friendly technology, has been recognized as an effective means of removing contaminants from water. Among the various photocatalysts, layered double hydroxides (LDHs), known as hydrotalcite-like materials, have been explored extensively in photocatalytic reactions due to their switchable properties and the large surface areas of their unique two-dimensional structures. In this article, recent advances in the photocatalytic degradation of emerging contaminants by LDH-based photocatalysts are reviewed. Firstly, the fundamental principles of the photocatalytic degradation of emerging contaminants using LDH-based materials are briefly introduced. Various LDHs applied in the photocatalytic degradation of emerging contaminants are broadly summarized into four types: pure-phase LDHs, interlayer-modified LDHs, LDH-based composites, and layered double oxides (LDOs). Moreover, the synthesis process and catalytic mechanism of LDH-based photocatalysts are also reviewed. An outlook on the problems and future development of LDH-based photocatalysts in water remediation is provided at the end.

Keywords: layered double hydroxides; photocatalysis; emerging contaminants; degradation



Citation: Luo, L.; Hou, C.; Wang, L.; Zhang, W.; Wang, C.; Liu, J.; Wu, Y.; Wang, C. Layered Double Hydroxide-Based Photocatalysts for the Removal of Emerging Contaminants: Progress in Past Ten Years. *Catalysts* **2024**, *14*, 252. <https://doi.org/10.3390/catal14040252>

Academic Editors: Daniele Dondi, Dhanalakshmi Vadivel and Andrea Speltini

Received: 15 March 2024

Revised: 30 March 2024

Accepted: 5 April 2024

Published: 11 April 2024



Copyright: © 2024 by the authors. Licensee MDPI, Basel, Switzerland. This article is an open access article distributed under the terms and conditions of the Creative Commons Attribution (CC BY) license (<https://creativecommons.org/licenses/by/4.0/>).

1. Introduction

With the current massive population growth and economic development, one of the most significant issues is the effect of pollution in the environment on human health [1]. Emerging contaminants (ECs), causing adverse effects on human health, have become a pressing issue for ecosystems in the water environment over the past few decades [2]. As a response, advanced oxidation processes (AOPs) are effective techniques for the treatment of emerging contaminants [3]. Advanced oxidation technologies include photochemical oxidation, catalytic wet oxidation, ozonation, electrochemical oxidation, and Fenton or Fenton-like oxidation, resulting in the generation of the hydroxyl radical ($\bullet\text{OH}$), hydrogen peroxide (H_2O_2), the superoxide radical ($\bullet\text{O}_2^-$), and singlet oxygen ($^1\text{O}_2$) to remove organic pollutants [4,5]. Among AOPs, photocatalytic oxidation is an eco-friendly, green, and sustainable technique for contaminant removal because it uses the Sun's energy [6,7]. Photocatalytic reactions are chemical reactions that convert light energy into chemical energy under the action of catalysts.

As promising photocatalysts, layered double hydroxides (LDHs) have attracted increasing attention in numerous fields, such as water treatment, CO_2 reduction, and water splitting, due to their supramolecular structures and specific properties [8–10]. Li and Zhang et al. found that LDH-based materials have received widespread attention in the field of photocatalysis and display significant application potential in the design and fabrication of photocatalysis due to the versatility in their compositions and architectures [11,12]. LDHs are known as hydrotalcite-like materials. All of the LDHs are widely defined by

the general molecular formula $[M_{(1-x)}^{2+}M_x^{3+}(\text{OH})_2]^{x+}(\text{A}^{n-})_{x/n} \cdot m\text{H}_2\text{O}$, where M^{2+} , M^{3+} , and A^{n-} represent divalent cations (e.g., Zn^{2+} , Cu^{2+} , Ni^{2+} , Mn^{2+} , Mg^{2+}), trivalent cations (e.g., Al^{3+} , Co^{3+} , Fe^{3+}), and anions (e.g., NO_3^- , Cl^- , CO_3^{2-} , SO_4^{2-} , PO_4^{3-}) [13–15]. LDHs are composed of layered two-dimensional (2D) sheets, and the structures of LDHs are similar to that of brucite ($\text{Mg}(\text{OH})_2$) [16–18], where the $-\text{OH}$ groups are hexagonally closely packed around magnesium cations to construct an octahedral structure, and the octahedral structures are stacked by sharing hydroxyl groups in each stacked sheet layer, in which the valences and charges are balanced (Figure 1). The structural unit of an octahedron consisting of one magnesium cation combined with six hydroxyl groups ($-\text{OH}$) is the most basic structural unit in brucite-like sheets [19]. The distinctive supramolecular structures of LDHs offer great potential in regulating and controlling energy levels at the quantum level due to the precisely controlled atomic compositions of the host and guest layers. When the trivalent cations are substituted for divalent cations, the host layers possess more positive charges to balance the negative charges of the guest layers. The charge density of the sheets can be managed by varying the M^{2+}/M^{3+} ratio, which affects the charge density of the interlayer gallery. Furthermore, LDHs can contain exchangeable interlayer anions [20–22].

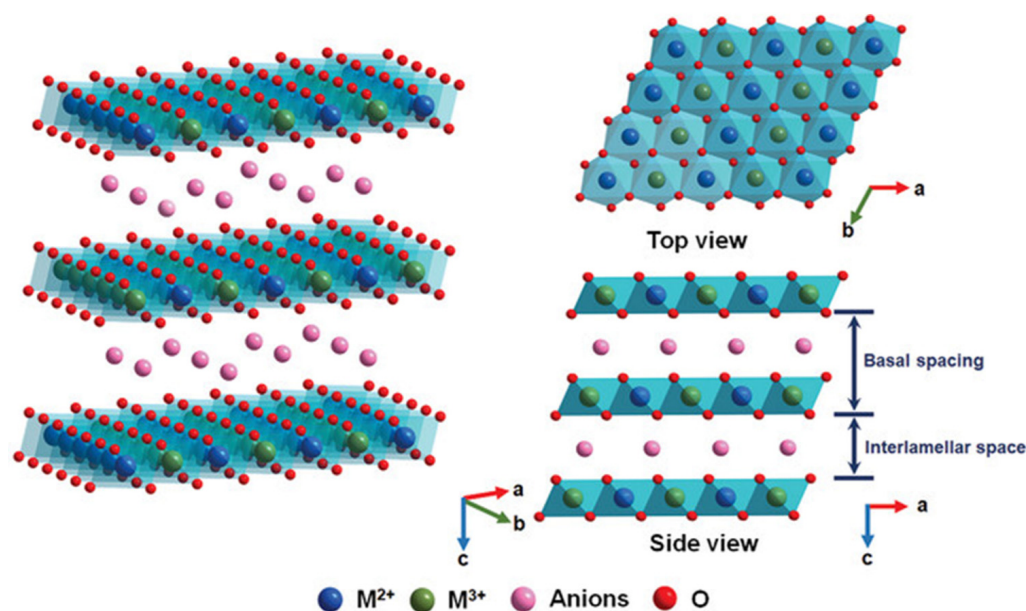


Figure 1. The crystalline structure of a layered double hydroxide (LDH) [8].

Electronic structures determine the properties of LDHs. Changes in the components of LDHs affect the energy gap, the redox potential of the conduction and valence bands, and the separation efficiency of hole–electron pairs [23]. First, in terms of the cations of the host layers, the elements in the sheets of LDHs can be replaced by any unsaturated metal (e.g., Zn, Fe, Co, or Ni), which helps to transfer electrons and enhance the light absorption [24,25], and any high-valence metal (e.g., Ti and Sn) can act as an electron trap to capture photoelectrons [26,27]. Among the various LDHs, ZnTi-LDHs, ZnCr-LDHs, and MgAl-LDHs are classical catalysts that exhibit fascinating photocatalytic performance, and the differences in their components cause marked variations in their energy gaps [28]. The doping of metal cations in sheets can enhance the photocatalyst’s properties by introducing charge defects and promoting charge separation [25,29]. The LDH-based ternary composites reviewed by Sun et al. all exhibited excellent photocatalytic performance, which was attributed to the enhanced electron–hole separation efficiency due to doping with metals [30]. Second, the anion located in the interlayer gallery can be exchanged as long as the anion does not dissolve the metal ions from the host layers [31]. Interlayer regions can offer molecular rendezvous points due to their high absorptivity. This contributes to the improvement of the photocatalytic performance. Third, interlayer

elements may combine with foreign elements to form heterogeneous structures on the surfaces of the host layers. Heterogeneous structures not only affect the structures of LDHs but also influence the photocatalytic performance. In this review, we focus on LDH-based photocatalysts for the removal of emerging contaminants from water (Figure 2). Figure 3 displays the number of published papers on the topics of “photocatalysis” and “LDH”. The number of papers published on contaminant removal has grown rapidly over the last decade, indicating that more and more researchers are being attracted to this area of science.

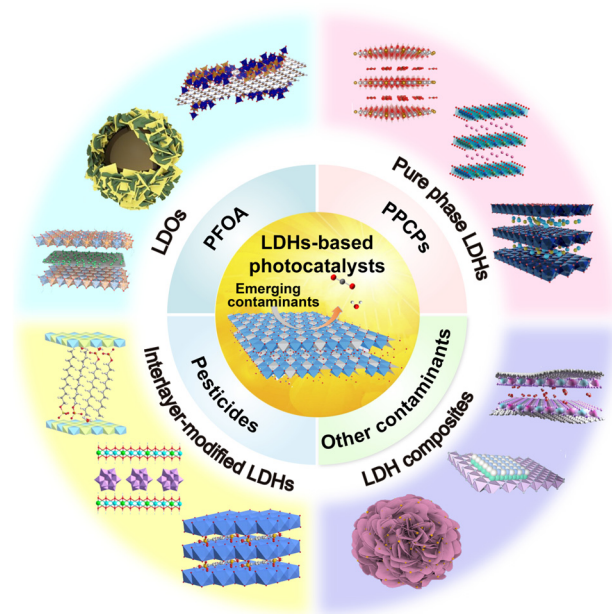


Figure 2. Schematic illustration of LDH-based photocatalysts for photocatalytic removal of emerging contaminants in water.

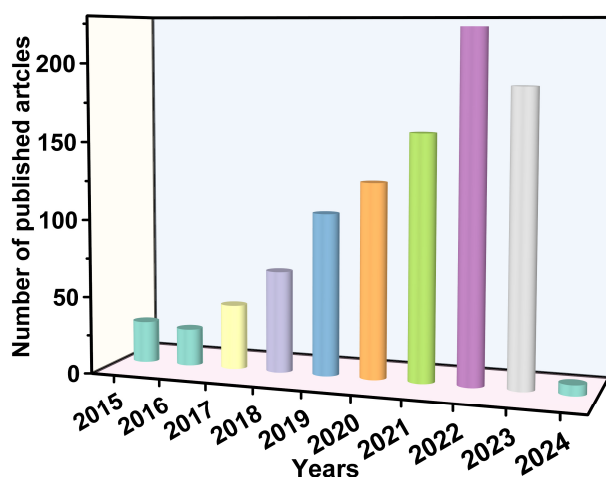


Figure 3. The number of published papers on photocatalysis and LDHs (literature search on the Web of Science database).

2. Fundamental Principles of Photocatalysis

Various LDHs take advantage of their own unique properties to produce active species under light excitation, which causes the non-selective mineralization of organic compounds [12]. The photocatalytic principles are based on the generation of the excited states of semiconducting materials by exposure to light [32]. In the structures of LDHs, an octahedral unit consisting of one metal cation that is combined with six hydroxyl groups can

serve as “a small semiconductor” [29,33,34]. In the excited state of an LDH, electrons (e^-) and holes (h^+) separate themselves from electron–hole pairs when the energy of a photon matches or exceeds the energy gap of the LDH [35]. Electrons from the valence band edge farther away rapidly fill the conduction band, and holes remain in the valence band. The excited electrons and holes subsequently migrate to the surfaces, and then the holes and electrons can interact with water and oxygen molecules on the surfaces of the catalyst, where oxidation reactions, mediated by holes, produce hydroxyl radicals, and the reduction reactions promoted by electrons convert molecular oxygen into superoxide radicals. The photocatalytic process involved in the mechanism of the photocatalytic production of active species is shown in Figure 4.

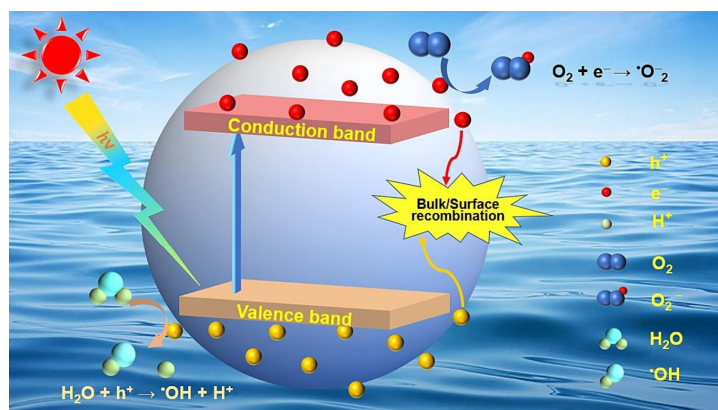


Figure 4. The LDH structure with interlayer sulfate anions [36].

Photocatalytic processes must promote photogenerated electron transfer to adsorbed particles provided that the potentials of the valence and conduction bands of the LDH suppress the redox potential of the adsorbed particles [33,37,38]. For oxidation or reduction, the potential of the valence band (versus the vacuum level) of the LDH must be more positive than the oxidation potential of the reactants serving as acceptors (versus a normal hydrogen electrode (NHE)), whereas the potential of the conduction band (versus the vacuum level) must be more negative than the reduction potential of the reactants serving as donors versus the NHE [39]. In brief, the redox potential of the adsorbed species must be located in the reaction region between the top of the valence band and the bottom of the conduction band of the LDH. The redox potentials of common active oxygen species are presented in Figure 5 [40,41].

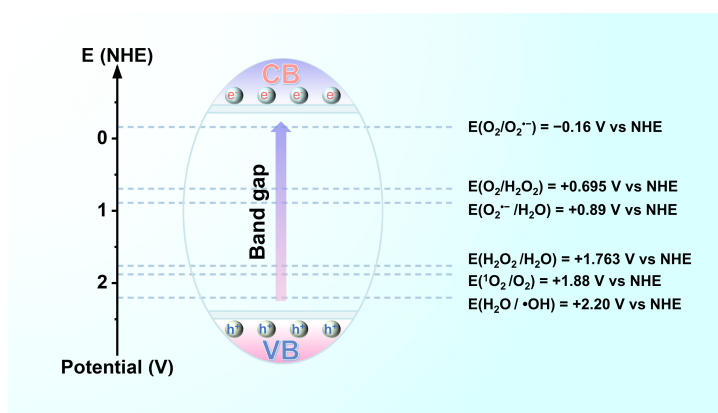


Figure 5. Potential regions of reaction in photocatalysis.

To utilize active species to completely mineralize organics, the photocatalysis must be enhanced by optimizing the electronic architectures of the LDHs. Photocatalysts should

meet the following requirements to exhibit good performance: (1) greater light absorption capacities in a wider light spectrum; (2) higher specific surface energies to attract sufficient molecules; (3) heterostructure or morphology features to improve the rate of photoinduced electron transition and to restrain the recombination of photogenerated carriers.

The component adjustment of LDHs is an important factor that affects the energy band and photocatalytic performance. First, in terms of the adjustment of the host sheets, there are various options for electronic architectures, if the metal elements or ratios of cations tend to change. For instance, when the Mg/Al ratio was varied from 2.0 to 3.5, the energy band gap changed from 1.265 to 3.321 eV in a chlorine intercalated MgAl-LDH according to DFT calculations. When Mg was replaced by Zn stepwise, the energy band gap changed from 3.85 to 5.43 eV, as calculated from the ultraviolet photoelectron spectroscopy (UPS) of a MgZnAl-CO₃-LDH. Second, some complexes with photocatalytic activity can be inserted into the interlaminar regions of LDHs, including inorganic anions, organic anions, metal complexes, and organic semiconductor materials. Third, composites of LDHs exhibit better photocatalytic behavior. The objects in the composites typically have a narrower band gap or act as the reactive center of the reaction, which can improve the photocatalytic performance. The complexes of LDHs can be divided into complexes with metal oxides, LDHs loaded with precious metals, self-assembled composites of LDHs with organic semiconductors, and mixed metal oxides (MMOs) obtained by calcining mixed crystal LDHs. These are discussed in detail in this review. The types of LDHs used for the photocatalytic degradation of organic pollutants are summarized in detail, including pure-phase LDHs and derivatives of LDHs. These derivatives are divided into LDHs modified in the interlayer space, composites based on LDHs, and derivatives of LDHs by calcination, for LDHs containing different elements. Table 1 summarizes the synthesis methods of LDH-based photocatalysts.

Table 1. Synthesis of LDH-based photocatalysts.

LDH	Fabrication Method	Condition	Ref.
Mn-doped ZnAl-LDHs	Co-precipitation	90 °C, 36 h	[42]
Ag/Zn-Al LDH	Mechanochemical operation	1200 rpm, 4 h	[43]
ZnNiFe-CO ₃ -LDHs	Complexing agent-assisted homogeneous precipitation technique	90 °C, 2 days	[44]
Mg/Al/Ti-LDH	Co-precipitation	room temperature, 24 h	[45]
MgAlSn-LDH	Co-precipitation	433 K, 36 h	[46]
Mn/Co/Ti-LDH	Hydrothermal	140 °C, 36 h	[47]
Co-Al LDH/GO	Co-precipitation	80 °C, 24 h	[48]
Ag@CN-LDH	Hydrothermal treatment	120 °C, 24 h	[49]
Mn/Ti-LDH	Hydrothermal	140 °C, 48 h	[50]
La-doped ZnCr-LDH	Co-precipitation	160 °C, 24 h	[51]
Pt/Zn-Ti-LDHs	Co-precipitation	100 °C, 24 h	[52]
CoAl-LDH/Bi ₂ MoO ₆	Hydrothermal	120 °C, 12 h	[53]
CoAl-LDH/g-C ₃ N ₄	Hydrothermal	110 °C, 9 h	[54]
Fe ₃ O ₄ @CuCr-LDH	Co-precipitation	60 °C, 24 h	[55]
TMU-5@Ni-Ti-LDH	Hydrothermal	110 °C, 24 h	[56]
g-C ₃ N ₄ /Ce-doped MgAl-LDH	Solvothermal	160 °C, 6 h	[57]

3. Pure-Phase LDHs

Today, a range of artificial LDHs with a pure single phase can be prepared [58]. Pure-phase LDHs only exist in the ratios of $M^{3+}/(M^{2+} + M^{3+})$ ranging from 0.2 to 0.33 [59]. The X-ray diffraction patterns (XRD) of pure-phase LDHs include (003), (006), (009), (110), and (113) characteristic reflections, and no other crystalline phases are detected in the spectrum [60,61].

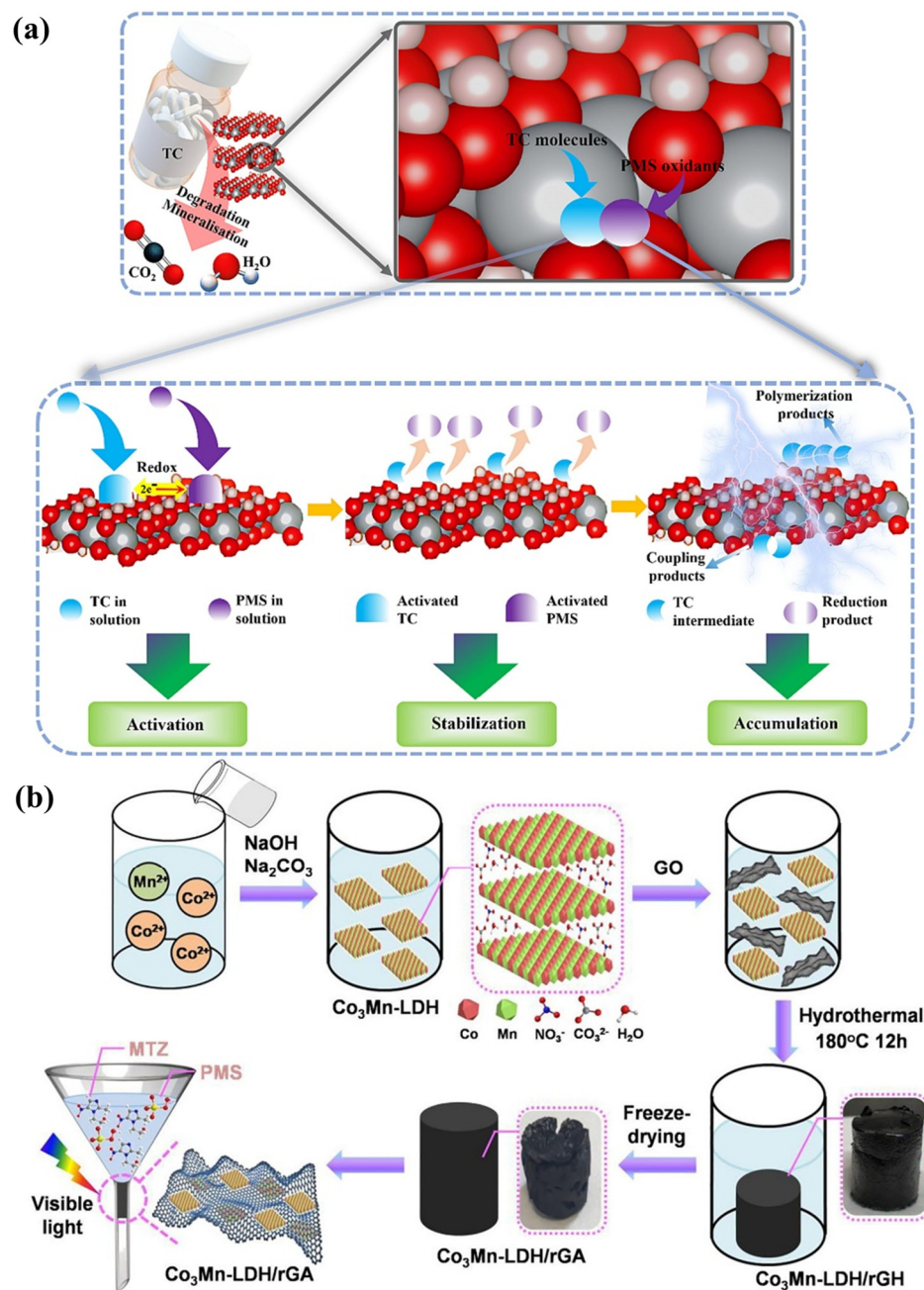


Figure 6. (a) Surface functional mechanism of DOTP for photocatalytic removal of TC by ZnAl-LDH [62]. (b) Fabrication and photocatalytic process of Co₃Mn-LDH/rGA in a recycling device [63].

Many LDH materials containing zinc have been studied previously, especially ZnAl-LDHs. A ZnAl-LDH was used as a photocatalyst to activate and stabilize the direct oxidative transfer process (DOTP) process on the surface of the catalyst (Figure 6a), which resulted in the complete removal of tetracycline hydrochloride (TC) within 35 min under visible light irradiation and a mineralization rate of up to 25% [62]. A zinc-iron-LDH (ZnFe-LDH) was synthesized by chemical co-precipitation and different anions were added to form a ZnFe-Cl⁻-LDH photocatalyst, and the concentration of dissolved zinc and iron in the water for five consecutive tests fulfilled the discharge standard [64]. A ZnTi-LDH prepared with urea in the homogeneous co-precipitation method showed the superior removal of colorless salicylic acid (SA) under visible light irradiation, which was much higher than that of commercial P25. The Zn²⁺ and Ti⁴⁺ cations were highly

dispersed on the brucite-like LDH sheets, effectively promoting charge separation and leading to excellent photocatalytic activity [65]. In addition, a ZnTi-LDH with a laminated architecture was deemed an effective and stable visible-light-induced photocatalyst [38,66].

Crystallite ZnAlTi-LDHs with M^{2+}/M^{3+} molar ratios (3:1) were fabricated using the simple co-precipitation method. Normally, M^{2+} would be replaced by M^{3+} to obtain the general formula $[Me_{1-x}^{2+}Me_x^{3+}(OH)_2]^{x+}(A^{n-})_{x/n} \bullet mH_2O$. The best degradation efficiency for diclofenac acid achieved was 93% after 120 min [67]. CuZnAl-LDHs with different Zn/Cu/Al ratios was manufactured by the co-precipitation method and were successfully applied for the photodegradation of naproxen (NPX) [68]. Compared to ZnAlTi-LDHs and CuZnAl-LDHs, ZnNiFe-LDHs exhibited greater light adsorption capabilities, lower band gaps, and good surface dispersion, producing remarkable photocatalytic performance without any pre-processing or calcination [44]. The entire photodegradation process occurred under visible light. These Zn-LDHs containing iron and nickel elements have high application value in the degradation of emerging contaminants. Moreover, LDHs containing magnesium, nickel, or cobalt also exhibit high visible light responses. MgAl-LDHs are also classical LDH materials. A simple impregnation-reduction method was used for the synthesis of a MgAl-LDH, which was applied for the degradation of ciprofloxacin (CIP) under visible light. Evidently, more than 77% of CIP was degraded within 50 min [69]. A MgAl-LDH with a Mg:Al molar ratio of 3:1 was synthesized by the co-precipitation method, which exhibited excellent photocatalytic degradation efficiency (65%) for the removal of diclofenac [70]. An innovative cobalt manganese material was prepared using a co-precipitation method, and the CoMn-LDHs exhibited excellent performance with the addition of peroxymonosulfate to deal with metronidazole (MTZ) under light irradiation (Figure 6b). Quenching experiments of free radicals revealed that $\bullet OH$ and $\bullet SO_4^-$ were produced in the CoMn-LDH/PMS system, and $\bullet SO_4^-$ was more reactive than $\bullet OH$ for the decomposition of MTZ [63]. All these LDHs containing cobalt lead to the superior stability of photocatalysts and visible light responses. Using a co-precipitation method, as-synthesized LDHs containing Ni displayed high photocatalytic activity (92.5%) for chlorpyrifos (CP) under visible light excitation [71].

4. Interlayer-Modified LDHs

The interlayer spaces of LDHs modified by inorganic or organic compounds such as inorganic anions, organic acids/bases, and organic complexes offer remarkable photocatalysts for organic contaminant removal [12]. They are usually synthesized by the calcination restructuring technique or the anionic exchange method. The inherent “memory effect” of LDHs produced by calcination allows them to rebuild themselves; in turn, LDHs with ionic compounds or organic compounds in the interlayer space are obtained [72]. Inorganic anions can be brought into the interlayer corridor through an anion exchange process employing corresponding salts. The positive layer structure can in turn store various negative anions in the interlayer gallery [73]. In addition, LDHs can also realize the intercalation of organics through organic self-assembly after exfoliation or in situ growth on organics, and these LDH materials modified by organics have shown strong interlacing interactions and adsorption capabilities towards organic contaminants [74–76].

The most common anions used for the intercalation of LDHs are oxyacid anions. Elhalil et al. presented ZnAl- CO_3^{2-} -LDH composites obtained via the co-precipitation method. The catalyst was used to efficiently remove caffeine from water [77]. ZnFe- SO_4^{2-} -LDH nanocomposites were also fabricated by a chemical co-precipitation process. Subsequent modification with graphene oxide generated a ZnFe- SO_4^{2-} -LDH/GO catalyst with ZnFe single bonds, and the degradation efficiency for ofloxacin (OFX) reached 71.19% after 150 min under light irradiation (Figure 7a) [64]. In addition, visible-light-responsive NiAl-LDH composites with MoS_4^{2-} were manufactured via solvent-free techniques (Figure 7b) [78]. All these LDHs modified by oxyacid anions or organic anions in the interlayer space show excellent photocatalytic performance.

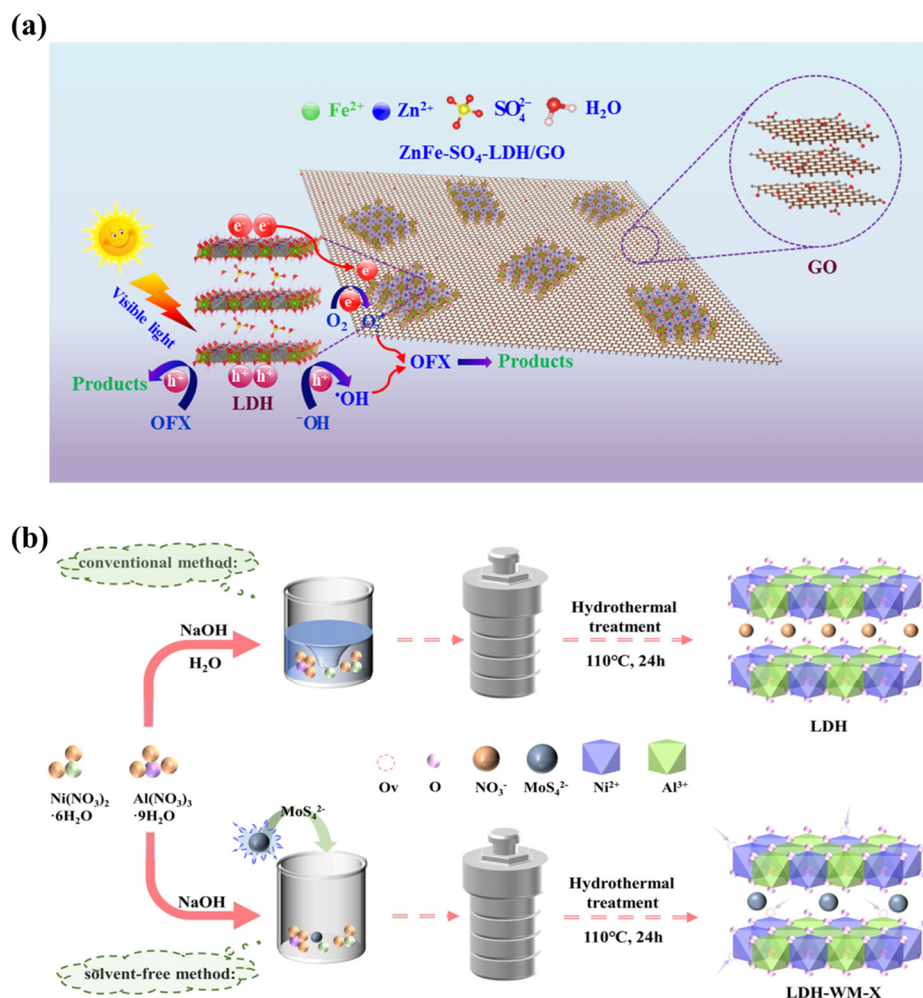


Figure 7. (a) The mechanism of OFX removal over ZnFe-SO_4^{2-} -LDH/GO photocatalysis [64]. (b) Schematic of the synthesis of NiAl-LDH and MoS_4^{2-} -NiAl-LDH [78].

Polyoxometalates (POMs) are a class of metal–oxygen cluster substances with sieve-like structures, and their photocatalytic activity originates from their unique structures [79,80]. POM-intercalated LDHs have attracted considerable attention due to the adjustable layer space and absorbability. POM–LDHs were first used as photocatalysts to decompose an aqueous solution of hexachlorocyclohexane (HCH) under mild conditions [81]. A novel polymetallic oxygenate (POM)-intercalated ZnAl–LDH was prepared by the aqueous ion exchange of the LDH precursor with the POM anion phosphomolybdic acid (PMA), which was subsequently used to degrade bisphenol A (BPA) in an aqueous solution [82]. Polyoxometalate-pillared Zn/Al/Mn–LDHs were rapidly manufactured by directly exchanging the anions. The as-prepared catalysts exhibited high photocatalytic degradation performance for aqueous organochlorine pesticides such as hexachlorocyclohexane through a first-order reaction [83].

An organometallic complex can also be inserted into LDHs. For instance, Tang et al. showed that ZnAl–LDH composites could be modified by an organic substance $[\text{FeEDTA}]^-$ in the interlayer gallery. These composites were synthesized by a convenient and effective anion exchange method. The maximum decolorization efficiency and TOC removal rate of the catalyst for azocarmine B (ACB) under optimal conditions could reach 97.27% and 90.36%, respectively [84]. CaAl–LDHs were heterogenized by inserting ferrate into the interlayer space. The LDHs intercalated by ferrate exhibited outstanding photocatalytic properties for phenol degradation via a heterogeneous photocatalysis mechanism [85]. All these ferric complexes exhibit increased adsorption and photocatalytic properties after intercalation.

5. LDH-Based Composites

LDH-based composites are fabricated from the recombination of primary LDHs with other photocatalytic materials, including inorganic semiconductors, organic polymers, quantum dots, and metal nanoparticles [86,87]. Composite hybrids possess new properties, and, hence, exhibit better photocatalytic properties. These high-performance composites can form photocatalytic heterostructures. Compared to single-phase elements as photocatalysts, LDH composites not only maintain the characteristics of each element, but also show enhanced photocatalytic properties through promoting the separation of photogenerated electron–hole pairs and extending the light absorption range.

During the past decade, titanium dioxide (TiO_2) has attracted great attention due to its excellent photochemical properties [88]. TiO_2 composite catalysts are being studied as promising photocatalysts due to their enhanced photocatalytic performance [89]. Numerous reports have covered the effects of LDH composites containing titanium dioxide on the photodegradation of organic pollutants. Nano-sized titanium dioxide supported on LDH composites ($\text{TiO}_2/\text{ZnAl-LDH}$, $\text{TiO}_2/\text{CuZnAl-LDH}$, $\text{TiO}_2/\text{ZnFe-LDH}$, and $\text{TiO}_2/\text{CuZnFeTi-LDH}$) was manufactured by convenient precipitation methods to disperse anatase titanium dioxide seed crystals on the surfaces of LDHs. The increased pore space and optical spectral characteristics were due to the modification of the titanium dioxide and the copper, trivalent iron, or tetravalent titanium cations in the layers of the LDHs. As a result, the as-prepared nanocomposites exhibited greater photocatalytic activity than P25 (TiO_2) [90]. In addition, an advanced strategy to improve the photocatalytic activity efficiency is to combine the LDHs with other functional units, and such units can be organic materials. Organic composite materials of LDHs exhibit the excellent photodegradation of pollutants. A $\text{Ti}_3\text{C}_2/\text{ZnTi-LDH@MXene}$ composite was prepared by the convenient hydrothermal method. The $\text{Ti}_3\text{C}_2/\text{ZnTi-LDH}$ based on MXene remarkably improved the adsorption of ibuprofen and the photocatalytic performance of $\text{Ti}_3\text{C}_2/\text{ZnTi-LDH@MXene}$ [91]. LDHs can also be combined with carriers to increase the specific surface areas. For example, ZnTi-LDH/h-BN composites were prepared by a convenient co-precipitation method and exhibited photocatalytic performance of 95% for diazepam (DZP) degradation under visible light, where the h-BN template was confirmed to be excellent carrier (Figure 8a) [92].

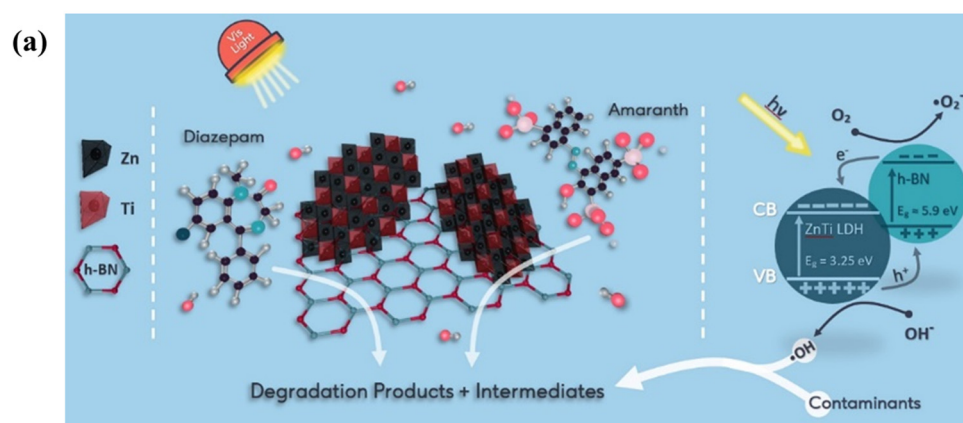


Figure 8. Cont.

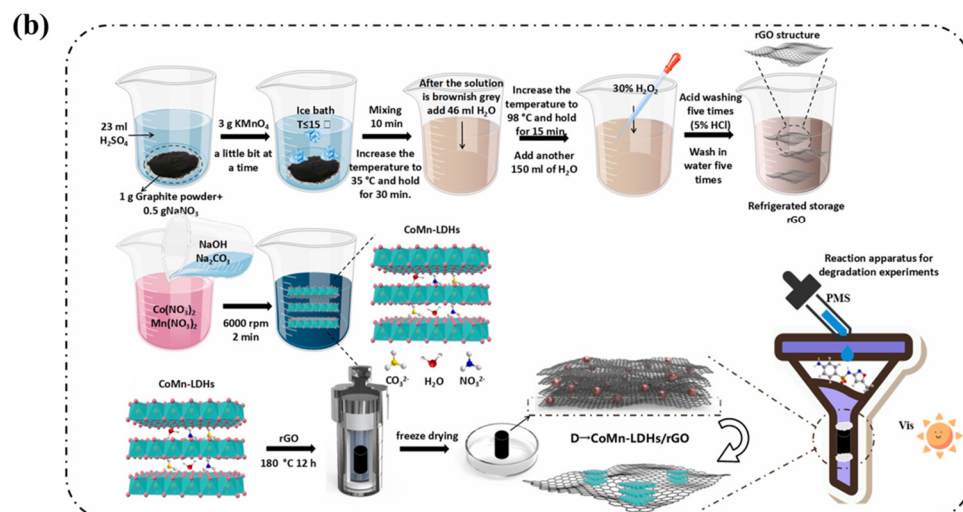


Figure 8. (a) Mechanism of diazepam degradation by ZnTi-LDH/h-BN [92]. (b) Preparation procedure of CoMn-LDH/rGO [93].

The combination of LDHs containing magnesium with metal oxides has become a hot spot in the field of photocatalysis. A novel $g-C_3N_4/MgZnAl-LDH$ ($M-CN/cLDH$) with a porous flower-like nanostructure was prepared by a template method, being self-assembled from laminated hybridized flakes. The efficient catalytic activity of the three-dimensional structure for antibiotics in seawater was ascribed to the synergistic effect of adsorption and photocatalysis [94]. Moreover, a series of innovative LDHs containing cobalt have been reported in recent years. A Zn-Co-LDH@biochar (Zn-Co-LDH@BC) was prepared via the hydrothermal method, where cobalt and zinc were uniformly dispersed on the surface of the biochar, and its specific surface area was significantly larger than that of the pristine BC. The excellent catalytic performance of the catalyst was attributed to the enhancement of the photogenerated carrier separation and the inhibition of the agglomeration of the LDH nanostructures by the addition of cobalt hydroxide and BC, respectively [95]. Three-dimensional CoMn-LDH/rGO composites were fabricated for the first time via a simple hydrothermal method, and the particular structure could help to improve the recycling efficiency of catalysts (Figure 8b) [93]. A novel two-dimensional stacked heterostructure, a direct Z-scheme, composed of oxygenic carbon nitride and ultrathin CoAl-LDH bridged by hydrogen bonds, was fabricated via in situ growth synthesis. The decomposition activity of the as-prepared complex was superior to that of oxygenic carbon nitride and an unmodified CoAl-LDH owing to the strong electronic coupling effect caused by the heterostructured interface. Moreover, the process of charge transfer in the Z-scheme heterostructure system may also occur with other LDHs with similar structures [96].

There have also been some recent reports on the application of new LDH materials containing nickel. A noble nanohybrid containing nickel, $Ni_2P/NiCo-LDH$, was manufactured by a simple calcination method, and the composites were more efficient photocatalysts than the unmodified NiAl-LDH. Unique Co-P bonds were formed in the material during the preparation process, which not only facilitated light absorption but also reduced the interfacial transfer resistance of the catalyst and improved its charge separation efficiency [97]. $Cs_{0.33}WO_3/NiAl-LDH$ composites were manufactured by a convenient solvothermal synthesis method and studied as photocatalysts to decompose tetracycline (TC) under visible light irradiation for the first time [98]. CoNi-LDH/ $ZnIn_2S_4$ was synthesized by a simple hydrothermal method, and the composite was a 1D/2D S-scheme heterojunction in which the bulk 1D CoNi nanowires were uniformly and densely anchored on the surfaces of the 2D ZIS nanosheets [99].

6. Layered Double Oxides (LDOs)

LDHs can be converted into layered double oxides (LDOs) after calcination at 300–600 °C, which not only maintains the topological properties of the LDHs but also results in better photocatalytic activity and greater adsorption capacities [100,101]. A significant feature of these calcined products is the “memory effect”, in which the collapsed structure can reconstruct the original layered structure after the adsorption of various anions [102].

A series of ZnAl–LDHs with various molar ratios of Zn to Al was calcined to prepare corresponding LDO composites by optimizing the synthesis parameters, and the adsorption properties for organic pollutants and the photocatalytic performance for photodegradation were explored. ZnAl–LDO carriers were obtained by calcining ZnAl–LDH at different temperatures, and subsequently Ag₂O/Ag nanoparticles were modified on the carriers to obtain Ag₂O–Ag/LDO, whose photocatalytic activity for TC degradation was related to the calcination temperature [103]. The Z-type ZnAl–LDO/Ag₂S heterojunction was constructed by electrostatic self-assembly and chemical deposition, in which LDO nanosheets were loaded on Ag₂S nanoparticles. The photocatalyst was found to have excellent structural and performance stability [104]. For further research on the ZnO–ZnAl₂O₄ system, ZnO–ZnAl₂O₄ materials with different cationic molar ratios (molar ratios = 1, 3 and 5) have been fabricated by calcination, and these exhibited superior photocatalytic decomposition activity towards caffeine (97.32%) in an aqueous solution, for which the dispersal of zinc oxide particles and the adsorption capacity were the most significant factors [105].

A series of MgAl–LDOs containing different amounts of B,N co-doping (MA#C(B,N)) were applied to the photodecomposition of TC in aqueous solutions. The photocatalytic efficiency of the MA#C(B,N) nanosheets was significantly higher than that of the LDO and BN [106]. During the catalyst synthesis process, Au³⁺ was reduced to Au nanoparticles in situ on the MgAl–LDH surface by utilizing the oxygen vacancies in the unique electronic environment, and finally Au/MgAl–LDH (Au/LDH) composites were formed (Figure 9a). The study of strong metal–vacancy interactions in composites provides new opportunities for the removal of cinnamyl alcohol from water [107]. Meanwhile, a MnFe–LDO was found to be useful for the photocatalytic degradation of pollutants in water. A simple co-precipitation–calcination technique was used to synthesize a low-cost MnFe–LDO–biochar photocatalyst with pronounced interconnected pores and folded edges, which correlated with the surface adsorption and photocatalytic performance of the catalyst [108]. A MnFe–LDO–biochar, prepared by the co-precipitation–calcination method, was also used for the photocatalytic degradation of TC. The catalyst had a large specific surface area and high photocurrent response, and the synergistic effect of the LDO and biochar was extremely prominent [109]. A three-dimensional flower-like cobalt-bearing layered double oxide/graphitic carbon nitride (Co–SLDO/CN) structure was prepared by sulfate anion induction, where the sulfate anions and the involvement of the calcination process induced the formation of oxygen vacancies (Figure 9b). Moreover, the incorporation of carbon nitride (CN) inhibited the aggregation of the Co–SLDH and provided it with nucleation sites [110].

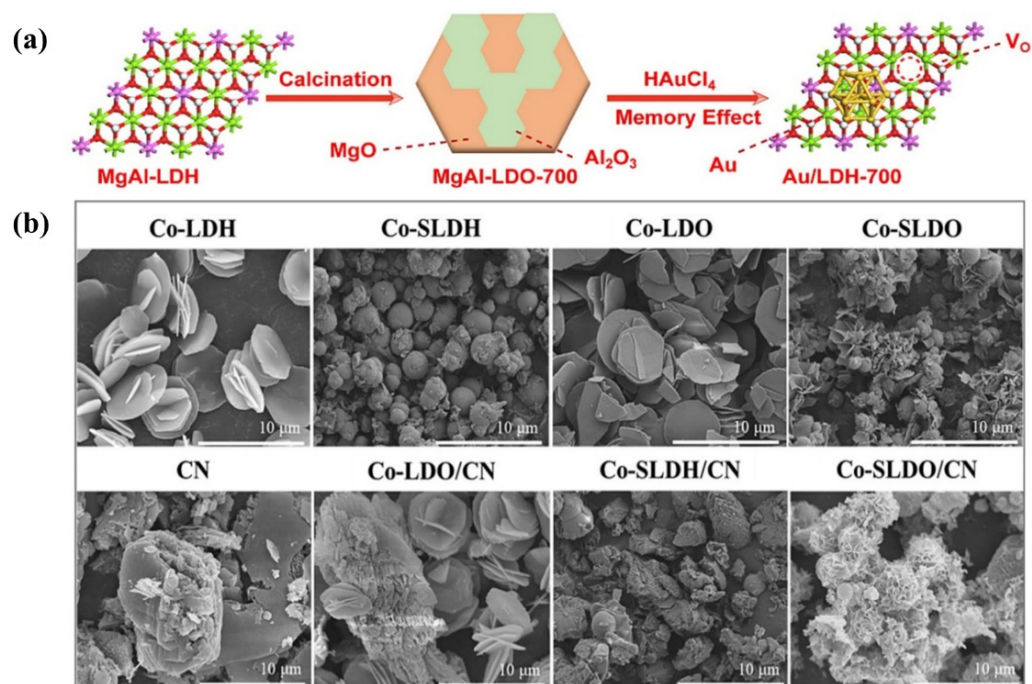


Figure 9. (a) The fabrication of Au/LDH-700 [107]. (b) SEM images of Co-LDH, Co-SLDH, Co-LDO, Co-SLDO, CN, Co-LDO/CN, Co-SLDH/CN, and Co-SLDO/CN [110].

7. LDH-Based Photocatalysts for Oxidative Degradation of Emerging Contaminants

Emerging organic pollutants such as pharmaceutical and personal care products (PPCPs), PFOA, and pesticides have serious impacts on human health and ecosystems, and it is critical to treat these pollutants using environmental technologies. LDH-based photocatalysts have been widely used to treat organic pollutants in water due to the flexible tenability, the dispersion of metals, and the chemical composition. Table 2 summarizes the research results on the removal of emerging pollutants by LDH-based photocatalytic materials during the last decade.

Table 2. Summary of LDH-based materials for photocatalytic removal of emerging contaminants.

Pollutant	LDH	Degradation Efficiency	Light Irradiation	Ref.
Ibuprofen	ZnFe-MMOs	95.7%, 90 min	500 W Xe lamp ($\lambda = 300$ nm)	[111]
Caffeine	ZnO-ZnAl ₂ O ₄	100%, 210 min	UV mercury lamp (400 W)	[105]
ACB	ZnAl-LDHs/[FeEDTA]	97.27%, 180 min	UV light	[84]
Caffeine	Ca/ZnO-Al ₂ O ₃	98.5%, 70 min	UV light	[112]
SA	ZnTi-LDH	65%, 6 h	250 W Xe lamp	[65]
Diethyl phthalate	Fe ₃ O ₄ @CuCr-LDH	70%, 120 min	solar simulator lamp ($\lambda > 400$ nm)	[55]
TC	In ₂ S ₃ /Zn-Al-LDHs	92.2%, 30 min	visible light ($\lambda > 400$ nm)	[113]
BPA	Bi ₂ MoO ₆ /Zn-Al-LDH	96%, 300 min	visible light	[114]
Lomefloxacin	Bi ₂ O ₃ /CuNiFe-LDHs	84.6%, 40 min	visible light (67 mW/cm ²)	[115]
CIP	M-RM/LDH	97.4%, 60 min	visible light ($\lambda = 380$ –780 nm)	[116]
TC	MgAl-LDH/ (BiO) ₂ CO ₃	97.2%, 105 min	visible light	[117]
Rifampicin	ZnCr-LDH/rGO	87.3%, 60 min	LED lamp	[118]
BPA	Cu/ZnO/CoFe-CLDH	80%, 6 h	visible light ($\lambda = 380$ –780 nm)	[119]
Rifampicin	ZnCr LDH/BC	100%, 40 min	LED lamp	[120]
CP	Co-Al-LDH/g-C ₃ N ₄ -CoFe ₂ O ₄	97.2%, 150 min	50 W LED lamp	[121]
NTP	Ag@AgCl/ZnAl-LDH	100%, 45 min	visible light (780 nm $>$ λ $>$ 420 nm)	[122]
NTP	Ag/Ag ₃ PO ₄ /Zn-Al-LDH	100%, 60 min	visible light (780 nm $>$ λ $>$ 420 nm)	[123]
NTP	Bi ₂ WO ₆ /Ag ₃ PO ₄ /Zn-Al-LDH	100%, 90 min	visible light (780 nm $>$ λ $>$ 420 nm)	[124]
NTP	Cu ₂ O/ZnAl-LDH	78%, 210 min	visible light ($\lambda > 420$ nm)	[125]

7.1. Photocatalytic Degradation of PPCPs

A wide variety of PPCPs are found in aquatic environments around the world due to the growing needs of livestock, agriculture, and disease treatment [126]. Misused PPCPs can enter the human body through bioconcentration and cause great harm to human health. LDH-based catalysts, as an important class of layered materials, are excellent candidates for the photocatalytic removal of PPCPs due to the synergistic effect of the active sites and exhibit exceptional catalytic activation capabilities.

Gao et al. synthesized uniformly dispersed NiAl–LDH/reduced graphene oxide (NiAlCe LDH/RGO) complexes with a large specific surface area, exhibiting excellent degradation efficiency for ciprofloxacin (CIP) under visible light irradiation (94%), which was significantly superior to that of the pristine NiAl–LDH (36%). The efficient catalytic ability of the composite was attributed to the fast photogenerated charge separation, caused by the presence of RGO and Ce [127]. In addition, highly crystalline TiO₂/ZnAl–LDH composites formed by synthesis after impregnation with TiO₂ exhibited catalytic photodegradation efficiency towards sulfamethoxazole (SMX) of more than 90% after five recycling experiments, in which •OH was the main reactive oxygen species in the degradation process [128]. Similarly, an aluminum-containing CoAl–LDH modified with N-doped carbon quantum dots (NCQDs), which was grown on hollow graphite carbon nitride spheres (HCNS) to form g–C₃N₄@LDH/NCQDs composites, exhibited superior degradation activity for TC than the pure LDH and HCNS under visible light. The hollow structure of the composite provided a generous number of active sites for the catalytic reaction, and the synergistic interaction between the multiple components facilitated the separation and transfer of the photogenerated carriers (Figure 10) [129].

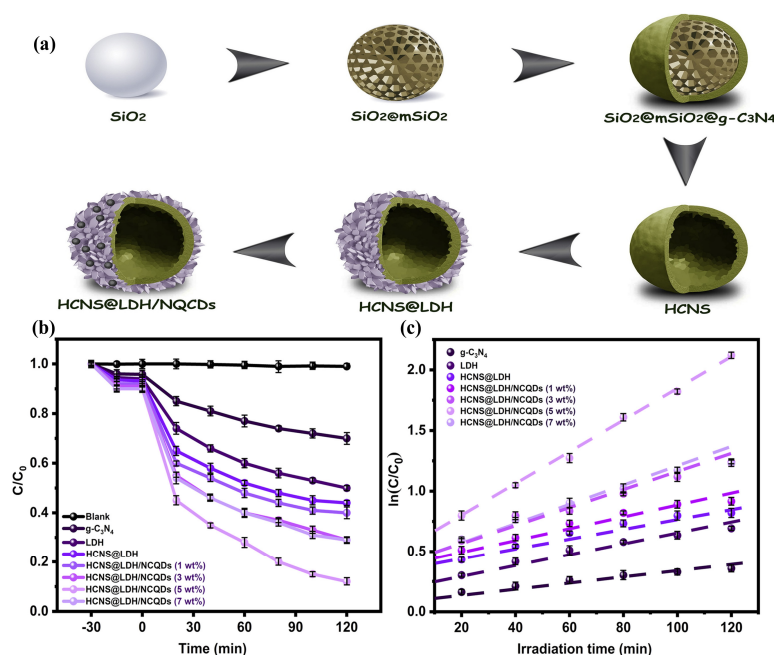


Figure 10. (a) Diagram of HCNS@LDH/NCQD heterojunction preparation. (b) TC photocatalytic degradation efficiency of prepared samples under visible light irradiation. (c) Kinetic curves for TC degradation over as-fabricated photocatalysts [129].

Xiong et al. [130] embedded Cu₂O nanoparticles onto the main laminate of a ZnTi–LDH by in situ reduction to form a CuZnTi–LDH, whose optoelectronic properties and photocatalytic degradation performance could be adjusted by varying the doping amount of Cu. UV–vis DRS spectra showed that the absorption peaks of the composites were significantly higher than that of the ZnTi–LDH when the (Cu²⁺/(Zn²⁺+Cu²⁺)) molar ratio was 0.10, suggesting that the doping of Cu₂O significantly improved the light-absorbing ability of the LDH. The results of a photoluminescence (PL) analysis showed the high

separation efficiency of the photogenerated electron–hole pairs in the composites. Ultimately, under visible light irradiation, the $\bullet\text{OH}$ -dominated reactive species produced by the CuZnTi–LDH degraded 71.6% of TC within 120 min, and the outstanding catalytic performance was attributed to the p–n heterostructure, which promoted the effective separation of electron–hole pairs and facilitated charge transfer.

7.2. Photocatalytic Degradation of Perfluorooctanoic Acid (PFOA)

Perfluorooctanoic acid (PFOA) is extensively applied in leather textiles, fire extinguishing agents, lubricants, and other industrial objects and is regarded as a persistent organic pollutant due to its stable chemical structure, high temperature resistance, and resistance to conventional treatment techniques [131,132]. The PFOA content in water should not be greater than 70 ng/L, based on the United States Environmental Protection Agency (USEPA) regulations [133]. PFOA has been found in drinking water and sewage and proven to be potentially toxic to animals and humans. Therefore, effective methods to remove PFOA from water are urgently needed.

Tang et al. synthesized a direct Z-scheme $\text{CeO}_2@/\text{NiAl-LDH}$ heterojunction, and the catalyst $\text{CeO}_2@/\text{NiAl-LDH}$ s possessed a core–shell structure (Figure 11) and could be used for the photocatalytic degradation of refractory PFOA. For example, 90.2% of PFOA could be degraded over the catalyst within 325 min at the reaction temperature of 45 °C, an initial pH of 9, and a catalyst dosage of 25 mg. Its degradation rate constant was $36.1 \text{ mg g}^{-1} \text{ h}^{-1}$ under a xenon lamp with an irradiation intensity of 500 W, which was much greater than that of NiAl–LDHs and CeO_2 . The authors suggested that the improved photocatalytic performance may have been due to the formation of an internal electric field that originated from the discrepancy in the phase work function of the CeO_2 and NiAl–LDHs, accelerating the transfer of electrons. They also conducted a detailed study of the degradation kinetics and thermodynamics and obtained details of the reaction order and rate equation. In addition, studies on the degradation pathways indicated that PFOA is eventually oxidized to carbon dioxide and water [134].

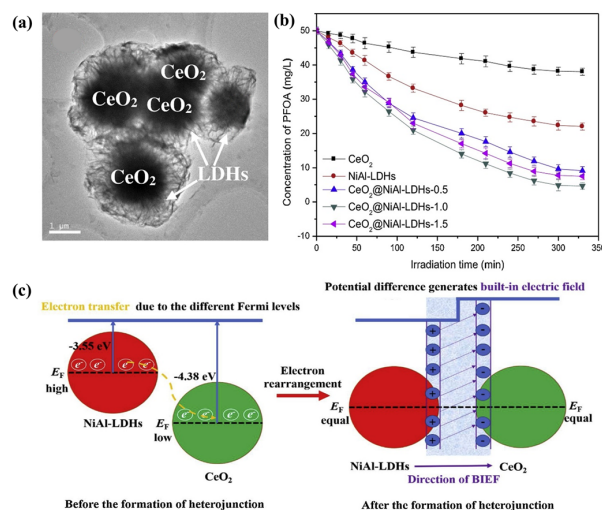


Figure 11. (a) TEM image of $\text{CeO}_2@/\text{NiAl-LDH}$ s. (b) Degradation efficiency of PFOA by different samples under visible light. (c) Illustration of charge transfer process and built-in electric field (BIEF) formation in $\text{CeO}_2@/\text{NiAl-LDH}$ heterojunction [134].

Yang et al. obtained flower-shaped microspheres of $\text{Bi}_5\text{O}_7\text{I}/\text{ZnO}$, which is an n–n heterojunction catalyst. The authors used zinc nitrate and aluminum nitrate as raw materials to first synthesize Zn–Al hydrotalcite, and then supported BiOI on the Zn–Al hydrotalcite to obtain the precursor $\text{BOI}_{0.04}\text{-BHZA}$. After further calcination at 400 °C, the final product $\text{Bi}_5\text{O}_7\text{I}/\text{ZnO}$ was obtained. They determined the optimal loading of BOI on hydrotalcite by performing PFOA degradation experiments. The formation of the n–n het-

erojunction expanded the photoresponse of the catalyst to the visible light region, improved the carrier separation efficiency, and thus led to excellent photocatalytic performance. Finally, $\text{Bi}_5\text{O}_7\text{I}/\text{ZnO}$ could remove about 91% of PFOA under visible light irradiation within 6 h, which was 2.4, 2.9, and 1.8 times higher than that of Zn–Al hydrotalcite, BiOI, and $\text{BiOI}_{0.04}\text{--BHZA}$. The active species removal experiments showed that the holes played a dominant role in the whole experimental process. Combined with the study of density functional theory, it was found that the holes mainly attacked the carboxyl groups of PFOA and decomposed the PFOA. The mechanism analysis showed that the rearrangement of the Fermi levels caused the conduction bands of ZnO to receive electrons from $\text{Bi}_5\text{O}_7\text{I}$, thereby promoting the separation of the photogenerated charge carriers [135]. Yang et al. prepared metal oxide–titanium dioxide (MMO– TiO_2). The degradation experiments showed that 300 mg/L of PFOA could be effectively removed, in an eco-friendly manner, within 240 min. This enhanced degradation rate was mainly due to an increase in the specific surface of the MMO– TiO_2 structures and a decrease in electron–hole recombination [136].

7.3. Photocatalytic Degradation of Pesticides

Pesticides are effective in controlling the quantity and quality of crops and eliminating pests in both agricultural and non-agricultural fields [137]. However, pesticide products are highly toxic and their irrational use can seriously threaten human health and even lead to poisoning [138]. LDHs have been used to treat pesticide residues in water bodies because of their ability to detect the specific properties of pesticides.

To effectively treat highly concentrated pesticides entering water sources, authors have used S-doped Ni–Co–LDHs modified by Fe_3O_4 nanoparticles to form S-doped Ni–Co LDH/ Fe_3O_4 composites, which were studied for the photocatalytic degradation of the pesticide CP. The experimental results showed that the k value (apparent rate constant) of S-doped Ni–Co LDH/ Fe_3O_4 was 0.018 min^{-1} , and the degradation rate of CP could reach 92.5% after 150 min when combined with the results of the experimental parameter investigation [71]. Sheikhpour et al. prepared the ternary catalyst Co–Al LDH// $g\text{--C}_3\text{N}_4\text{--CoFe}_2\text{O}_4$, which was also used for the degradation of CP under visible light (97.2%), and the catalytic activity of the composites was significantly higher than that of the pure-phase $g\text{--C}_3\text{N}_4$ and CoFe_2O_4 . The results of the capture experiments confirmed that $\bullet\text{OH}$ was the main active species for CP degradation in the photocatalytic process, and the degradation of CP could still reach 80% after five cycles [121]. Zheng et al. fabricated Cu_2O intercalated ZnAl–LDH ($\text{Cu}_2\text{O}/\text{ZnAl}\text{--LDH}$) photocatalysts by a hydrothermal method, which could completely degrade nitenpyram (NTP) in 210 min and had a mineralization rate of 40%. In addition, the photocatalyst had some bactericidal effects and treatment potential for waste leachates. It was shown that the efficient catalytic activity was attributed to the synergistic effect of the intercalation structure and the crystal surface [125].

S-scheme heterojunction construction has been considered as a promising strategy to improve the photocatalytic performance. $\text{Bi}_2\text{WO}_6/\text{Ag}_3\text{PO}_4/\text{Zn}\text{--Al}\text{--LDH}$ heterojunctions, synthesized by Zheng et al., with a reef-like morphology, were used to treat NTP in water. Interestingly, the uniformly distributed coral reef structure facilitated the enhancement of the photocatalytic activity, and the heterogeneous structure effectively extended the carrier lifetime. The directional transfer of photogenerated electrons due to the internal electric field promoted the efficient separation and transport of the carriers, thus presenting remarkable photocatalytic degradation capabilities. Eventually, the $\bullet\text{O}_2^-$ and h^+ generated in the photocatalytic system enabled the S-scheme heterojunction to completely degrade 50 mg/L of NTP in 90 min (Figure 12) [124].

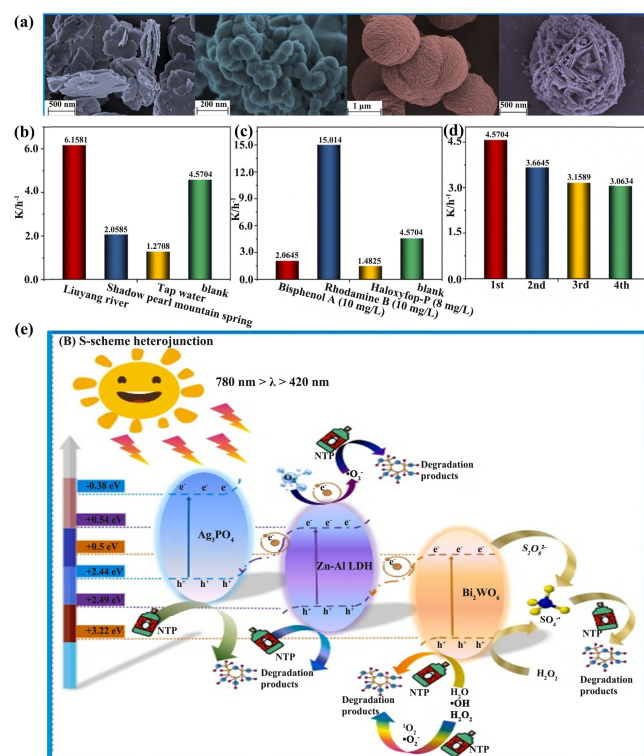


Figure 12. (a) SEM images of Zn–Al–LDH, Ag₃PO₄, Bi₂WO₆, BWLDH0.3, and AP0.5BWLDH0.3. The k-value of the AP0.5BWLDH0.3/PMS/Vis system for the removal of (b) NTP in simulated natural water and (c) other typical organic pollutants. (d) The k-value for the cyclic degradation of the AP0.5BWLDH0.3/PMS/Vis system. (e) The mechanics of photocatalysis in the AP0.5BWLDH0.3/PMS/Vis system [124].

7.4. Photocatalytic Segradation of Other Contaminants

The presence of emerging contaminants such as endocrine-disrupting chemicals (EDCs) and microplastics (MPs) has received a great deal of attention. Nonylphenol (NP) is a nonionic surfactant and a typical EDC pollutant that is widely used in industrial products such as ink and latex paint. Due to the wide application of NP, it is easily introduced into water, but NP is not easily degraded [136,139,140]. Therefore, powerful techniques need to be developed to remove NP. Arjomandi-Behzad et al. constructed a core–shell cocatalyst consisting of nitrogen-doped hollow carbon spheres (N–HCS) as the core and LDH nanoplates as the photoactive shell. As the supporter of an LDH, N–HCS could effectively prevent the agglomeration of particles, increased the specific surface area of the catalyst, and improved the electron transfer rate as an electron transfer channel, leading to boosted photocatalytic performance. As expected, the LDH@N–HCS (15 wt%) degraded 85% of NP at 180 min. The author claimed that there were four reasons for the improved activity of the catalyst: (1) the core–shell structure promoted carrier separation; (2) the addition of the LDH increased the specific surface area of the catalyst, which provided more reachable active sites for the degradation of pollutants; (3) the hollow structure enhanced the capture of light by the photocatalyst; (4) N–HCS promotes charge transfer as an electron reservoir [141].

MPs is a general term for plastic fragments with a particle size of less than 5 mm, mainly including polyethylene, polypropylene, and so on. MPs accumulate in water and migrate to various places with the flow of the water, and they can enrich heavy metal ions in water due to their large specific surface area. Additionally, MPs accompanied by heavy metals can easily enter the human body and cause harm to human health [142,143]. Jiang et al. prepared a CuMgAlTi–R400 composite photomaterial for the photocatalytic degradation of polystyrene and polyethylene. They found that the particle sizes of polystyrene and

polyethylene decreased by 54.2% and 33.7% after visible light irradiation. The decrease in the particle size of the pollutants is beneficial as it increases the degradation rate. The results of the EPR analysis showed that the hydroxyl radical and superoxide radical contributed to the decomposition of polystyrene and polyethylene. This study provides a feasible strategy for the effective control of MPs (Figure 13) [144].

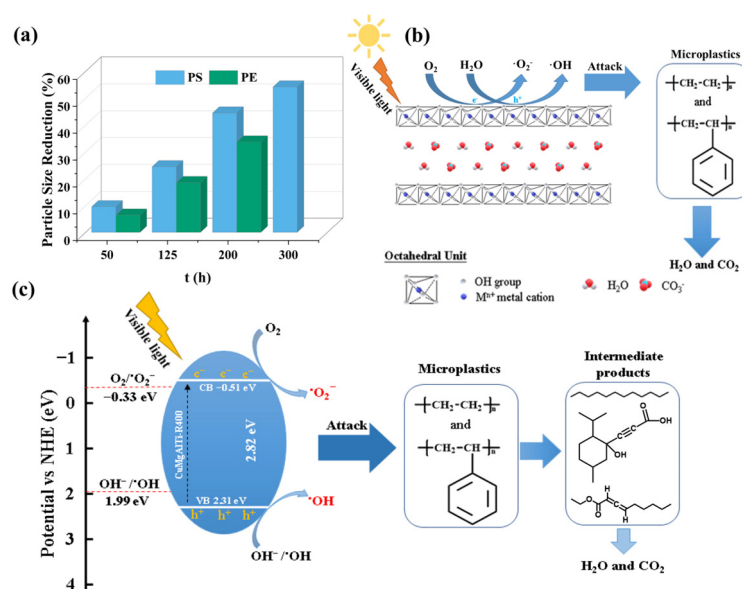


Figure 13. (a) Percentage size reduction of microplastic particles with exposure time. (b) Mechanism of MP degradation on CuMgAlTi-R400 surface. (c) Mechanism of MP degradation by CuMgAlTi-R400 irradiation in visible light [144].

8. Conclusions

In summary, this review describes the synthesis strategies of LDH-based photocatalysts and the progress of their application in the field of photocatalytic degradation for emerging contaminants over the past decade. A series of LDH-based photocatalysts with synergistic effects can be obtained by the functional modification of pure-phase LDHs through interlayer modification, surface compounding, and calcination. These LDH-based photocatalysts, with excellent electronic structures and crystal structures, can effectively remove emerging contaminants from water. Overall, these LDH-based photocatalysts have superior degradation activity due to the following characteristics: high light absorption, wide optical absorption ranges, and high separation efficiency of holes and electrons. Although LDH-based photocatalysts have shown exciting progress in the treatment of emerging contaminants, there still remain several pressing challenges, notably the following: (1) the development of low-cost catalysts for the efficient treatment of pollutants is necessary; (2) besides the treatment of PPCPs, LDH-based photocatalysts should be used towards the photocatalytic degradation of other emerging contaminants (e.g., PFOA, EDCs, nicotine, caffeine, etc.); (3) the degradation pathways and intermediate product toxicity for emerging contaminants should be studied in detail, and attention should be paid to the degree of mineralization of pollutants in LDH-based photocatalytic systems; and (4) the development of LDH-based catalysts for practical application in the photocatalytic degradation of emerging contaminants requires further research.

Author Contributions: Writing—original draft preparation, L.L. and C.H.; writing—review and editing, C.H. and W.Z.; visualization, C.W. (Cong Wang); resources, J.L.; data curation, Y.W.; writing—review and editing, L.W.; funding acquisition, L.W.; supervision, L.W. and C.W. (Chuanyi Wang). All authors have read and agreed to the published version of the manuscript.

Funding: This work was funded by the financial support of the National Natural Science Foundation of China (Grant No. 22076114 and U1703129), the Key Research and Development Program of Shaanxi (2021SF-452), and the “Thousand Talents Program” of Shaanxi Province of China.

Data Availability Statement: No new data were created or analyzed in this study. Data sharing is not applicable to this article.

Conflicts of Interest: The authors declare no conflicts of interest.

References

1. Zhan, Q.-N.; Shuai, T.-Y.; Xu, H.-M.; Zhang, Z.-J.; Li, G.-R. Recent advances in the regulation of the coordination structures and environment of single-atom catalysts for carbon dioxide reduction reaction. *J. Mater. Chem. A* **2023**, *11*, 7949–7986. [[CrossRef](#)]
2. Gao, Y.; Niu, X.; Wang, M.; Li, G.; An, T. An inescapable fact: Toxicity increase during photo-driven degradation of emerging contaminants in water environments. *Curr. Opin. Green Sustain. Chem.* **2021**, *30*, 100472. [[CrossRef](#)]
3. Shang, Y.; Xu, X.; Gao, B.; Wang, S.; Duan, X. Single-atom catalysis in advanced oxidation processes for environmental remediation. *Chem. Soc. Rev.* **2021**, *50*, 5281–5322. [[CrossRef](#)]
4. Miklos, D.B.; Remy, C.; Jekel, M.; Linden, K.G.; Drewes, J.E.; Hubner, U. Evaluation of advanced oxidation processes for water and wastewater treatment—A critical review. *Water Res.* **2018**, *139*, 118–131. [[CrossRef](#)]
5. Wang, J.; Wang, S. Reactive species in advanced oxidation processes: Formation, identification and reaction mechanism. *Chem. Eng. J.* **2020**, *401*, 126158. [[CrossRef](#)]
6. Wang, L.; Zhu, Z.; Wang, F.; Qi, Y.; Zhang, W.; Wang, C. State-of-the-art and prospects of Zn-containing layered double hydroxides (Zn-LDH)-based materials for photocatalytic water remediation. *Chemosphere* **2021**, *278*, 130367. [[CrossRef](#)]
7. Wang, C.; Shi, P.; Wang, Z.; Guo, R.; You, J.; Zhang, H. Efficient wastewater disinfection through FeOOH-mediated photo-Fenton reaction: A review. *J. Environ. Chem. Eng.* **2023**, *11*, 111269. [[CrossRef](#)]
8. Wang, Y.; Zhang, M.; Liu, Y.; Zheng, Z.; Liu, B.; Chen, M.; Guan, G.; Yan, K. Recent advances on transition-metal-based layered double hydroxides nanosheets for electrocatalytic energy conversion. *Adv. Sci.* **2023**, *10*, 2207519. [[CrossRef](#)]
9. Yu, J.; Yu, F.; Yuen, M.-F.; Wang, C. Two-dimensional layered double hydroxides as a platform for electrocatalytic oxygen evolution. *J. Mater. Chem. A* **2021**, *9*, 9389–9430. [[CrossRef](#)]
10. Zhu, Z.; Wang, L.; Zhang, W.; Hou, C.; Wang, C.; Zhao, J. Ultrathin CuNi₂Al-LDH nanosheets with enhanced electron transfer for visible-light-driven photo-Fenton-like water decontamination. *Chem. Eng. J.* **2024**, *481*, 148313. [[CrossRef](#)]
11. Li, C.; Wei, M.; Evans, D.G.; Duan, X. Layered double hydroxide-based nanomaterials as highly efficient catalysts and adsorbents. *Small* **2014**, *10*, 4469–4486. [[CrossRef](#)]
12. Zhang, G.; Zhang, X.; Meng, Y.; Pan, G.; Ni, Z.; Xia, S. Layered double hydroxides-based photocatalysts and visible-light driven photodegradation of organic pollutants: A review. *Chem. Eng. J.* **2020**, *392*, 123684. [[CrossRef](#)]
13. Prestopino, G.; Pezzilli, R.; Calavita, N.J.; Leonardi, C.; Falconi, C.; Medaglia, P.G. Layered-Double-Hydroxide (LDH) pyroelectric nanogenerators. *Nano Energy* **2023**, *118*, 109017. [[CrossRef](#)]
14. Veeralingam, S.; Gunasekaran, S.S.; Badhulika, S. Bifunctional NiFe LDH as a piezoelectric nanogenerator and asymmetric pseudo-supercapacitor. *Mater. Chem. Front.* **2022**, *6*, 2297–2308. [[CrossRef](#)]
15. Zhang, Q.; Zhang, G.; Huang, Y.; He, S.; Li, Y.; Jin, L.; Han, J. Surface-modified LDH nanosheets with high dispersibility in oil for friction and wear reduction. *ACS Appl. Mater. Interfaces* **2024**, *16*, 5316–5325. [[CrossRef](#)]
16. Mohapatra, L.; Parida, K. A review on the recent progress, challenges and perspective of layered double hydroxides as promising photocatalysts. *J. Mater. Chem. A* **2016**, *4*, 10744–10766. [[CrossRef](#)]
17. ten Elshof, J.E.; Yuan, H.; Gonzalez Rodriguez, P. Two-dimensional metal oxide and metal hydroxide nanosheets: Synthesis, controlled assembly and applications in energy conversion and storage. *Adv. Energy Mater.* **2016**, *6*, 1600355. [[CrossRef](#)]
18. Varadwaj, G.B.B.; Oyetade, O.A.; Rana, S.; Martincigh, B.S.; Jonnalagadda, S.B.; Nyamori, V.O. Facile synthesis of three-dimensional Mg–Al layered double hydroxide/partially reduced graphene oxide nanocomposites for the effective removal of Pb²⁺ from aqueous solution. *ACS Appl. Mater. Interfaces* **2017**, *9*, 17290–17305. [[CrossRef](#)]
19. Nayak, S.; Kumar Das, K.; Parida, K. Indulgent of the physiochemical features of MgCr-LDH nanosheets towards photodegradation process of methylene blue. *J. Colloid Interface Sci.* **2023**, *634*, 121–137. [[CrossRef](#)]
20. Wang, Q.; O’Hare, D. Recent advances in the synthesis and application of layered double hydroxide (LDH) nanosheets. *Chem. Rev.* **2012**, *112*, 4124–4155. [[CrossRef](#)]
21. Goh, K.-H.; Lim, T.-T.; Dong, Z. Application of layered double hydroxides for removal of oxyanions: A review. *Water Res.* **2008**, *42*, 1343–1368. [[CrossRef](#)]
22. Pan, Y.; Du, J.; Chen, J.; Lian, C.; Lin, S.; Yu, J. Interlayer intercalation of Li/Al-LDHs responsible for high-efficiency boron extraction. *Desalination* **2022**, *539*, 115966. [[CrossRef](#)]
23. Xu, J.; Li, Q.; Liu, X.; Yang, Q. P-doped nanorod MoO₃ and nanoflower NiAl-LDH construct S-type heterojunction for photocatalytic high-efficiency hydrogen evolution. *Surf. Interfaces* **2023**, *43*, 103593. [[CrossRef](#)]
24. Liu, P.F.; Yang, S.; Zhang, B.; Yang, H.G. Defect-rich ultrathin cobalt–iron layered double hydroxide for electrochemical overall water splitting. *ACS Appl. Mater. Interfaces* **2016**, *8*, 34474–34481. [[CrossRef](#)]

25. Xu, J.; Liu, X.; Zhou, Z.; Deng, L.; Liu, L.; Xu, M. Surface defects introduced by metal doping into layered double hydroxide for CO₂ photoreduction: The effect of metal species in light absorption, charge transfer and CO₂ reduction. *Chem. Eng. J.* **2022**, *442*, 136148. [[CrossRef](#)]
26. Zhao, Y.; Jia, X.; Chen, G.; Shang, L.; Waterhouse, G.I.; Wu, L.-Z.; Tung, C.-H.; O'Hare, D.; Zhang, T. Ultrafine NiO nanosheets stabilized by TiO₂ from monolayer NiTi-LDH precursors: An active water oxidation electrocatalyst. *J. Am. Chem. Soc.* **2016**, *138*, 6517–6524. [[CrossRef](#)]
27. Dvininov, E.; Ignat, M.; Barvinschi, P.; Smithers, M.; Popovici, E. New SnO₂/MgAl-layered double hydroxide composites as photocatalysts for cationic dyes bleaching. *J. Hazard. Mater.* **2010**, *177*, 150–158. [[CrossRef](#)]
28. Liang, W.; Zhang, X.; Wang, C.; Bai, J.; Li, X.; Mao, Y.; Cai, J.; Li, Y.; Chang, S.; Xu, Z.; et al. Visible-light-driven tetracycline hydrochloride degradation via ZnTi-LDHs/Ce₂S₃ Z-scheme heterojunctions: Performance and mechanistic analysis. *J. Environ. Chem. Eng.* **2024**, *12*, 111997. [[CrossRef](#)]
29. Ali Khan, A.; Tahir, M.; Khan, N. LDH-based nanomaterials for photocatalytic applications: A comprehensive review on the role of bi/trivalent cations, anions, morphology, defect engineering, memory effect, and heterojunction formation. *J. Energy Chem.* **2023**, *84*, 242–276. [[CrossRef](#)]
30. Sun, H.; Heo, Y.-J.; Park, J.-H.; Rhee, K.Y.; Park, S.-J. Advances in layered double hydroxide-based ternary nanocomposites for photocatalysis of contaminants in water. *Nanotechnol. Rev.* **2020**, *9*, 1381–1396. [[CrossRef](#)]
31. Cao, Y.; Zheng, D.; Zhang, F.; Pan, J.; Lin, C. Layered double hydroxide (LDH) for multi-functionalized corrosion protection of metals: A review. *J. Mater. Sci. Technol.* **2022**, *102*, 232–263. [[CrossRef](#)]
32. Rauf, M.A.; Ashraf, S.S. Fundamental principles and application of heterogeneous photocatalytic degradation of dyes in solution. *Chem. Eng. J.* **2009**, *151*, 10–18. [[CrossRef](#)]
33. Bian, X.; Zhang, S.; Zhao, Y.; Shi, R.; Zhang, T. Layered double hydroxide-based photocatalytic materials toward renewable solar fuels production. *InfoMat* **2021**, *3*, 719–738. [[CrossRef](#)]
34. Feng, H.; Yu, J.; Tang, L.; Wang, J.; Dong, H.; Ni, T.; Tang, J.; Tang, W.; Zhu, X.; Liang, C. Improved hydrogen evolution activity of layered double hydroxide by optimizing the electronic structure. *Appl. Catal. B Environ.* **2021**, *297*, 120478. [[CrossRef](#)]
35. Mohapatra, L.; Parida, K.M. Dramatic activities of vanadate intercalated bismuth doped LDH for solar light photocatalysis. *Phys. Chem. Chem. Phys.* **2014**, *16*, 16985–16996. [[CrossRef](#)] [[PubMed](#)]
36. Luo, J.; Li, W.; Yin, R.; Liu, Q.; Xin, X.; Yang, L.; He, K.; Ma, D.; Lv, S.; Xing, D. Photocatalyst degradation of perfluorooctanoic acid in water: Mechanisms, approaches, and perspectives. *Sep. Purif. Technol.* **2024**, *338*, 126503. [[CrossRef](#)]
37. Boumeriame, H.; Da Silva, E.S.; Cherevan, A.S.; Chafik, T.; Faria, J.L.; Eder, D. Layered double hydroxide (LDH)-based materials: A mini-review on strategies to improve the performance for photocatalytic water splitting. *J. Energy Chem.* **2022**, *64*, 406–431. [[CrossRef](#)]
38. Zou, J.; Wang, Z.; Guo, W.; Guo, B.; Yu, Y.; Wu, L. Photocatalytic selective oxidation of benzyl alcohol over ZnTi-LDH: The effect of surface OH groups. *Appl. Catal. B Environ.* **2020**, *260*, 118185. [[CrossRef](#)]
39. Guru, S.; Kumar, S.; Bellamkonda, S.; Gangavarapu, R.R. Synthesis of CuTi-LDH supported on g-C₃N₄ for electrochemical and photoelectrochemical oxygen evolution reactions. *Int. J. Hydrogen Energy* **2021**, *46*, 16414–16430. [[CrossRef](#)]
40. He, W.; Jia, H.; Wamer, W.G.; Zheng, Z.; Li, P.; Callahan, J.H.; Yin, J.-J. Predicting and identifying reactive oxygen species and electrons for photocatalytic metal sulfide micro–nano structures. *J. Catal.* **2014**, *320*, 97–105. [[CrossRef](#)]
41. Li, Y.; Zhang, W.; Niu, J.; Chen, Y. Mechanism of photogenerated reactive oxygen species and correlation with the antibacterial properties of engineered metal-oxide nanoparticles. *ACS Nano* **2012**, *6*, 5164–5173. [[CrossRef](#)]
42. Morales-Mendoza, G.; Tzompantzi, F.; García-Mendoza, C.; López, R.; De la Luz, V.; Lee, S.-W.; Kim, T.-H.; Torres-Martínez, L.M.; Gómez, R. Mn-doped Zn/Al layered double hydroxides as photocatalysts for the 4-chlorophenol photodegradation. *Appl. Clay Sci.* **2015**, *118*, 38–47. [[CrossRef](#)]
43. Li, Z.; Zhang, Q.; Liu, X.; Wu, L.; Hu, H.; Zhao, Y. One-step mechanochemical synthesis of plasmonic Ag/Zn–Al LDH with excellent photocatalytic activity. *J. Mater. Sci.* **2018**, *53*, 12795–12806. [[CrossRef](#)]
44. Dang, R.; Ma, X.; Liu, J.; Yan, L.; Gao, W.; Li, J.; Chen, B. Preparation of Zn²⁺–Ni²⁺–Fe³⁺–CO₃²⁻ LDHs and study of photocatalytic activities for decomposition of Methyl Orange solution. *Compos. Interfaces* **2016**, *24*, 1–11. [[CrossRef](#)]
45. Hosni, K.; Abdelkarim, O.; Frini-Srasra, N.; Srasra, E. Synthesis, structure and photocatalytic activity of calcined Mg–Al–Ti-layered double hydroxides. *Korean J. Chem. Eng.* **2014**, *32*, 104–112. [[CrossRef](#)]
46. Mancipe, S.; Tzompantzi, F.; Rojas, H.; Gómez, R. Photocatalytic degradation of phenol using MgAlSn hydrotalcite-like compounds. *Appl. Clay Sci.* **2016**, *129*, 71–78. [[CrossRef](#)]
47. Roy Chowdhury, P.; Bhattacharyya, K.G. Synthesis and characterization of Mn/Co/Ti LDH and its utilization as a photocatalyst in visible light assisted degradation of aqueous Rhodamine B. *RSC Adv.* **2016**, *6*, 112016–112034. [[CrossRef](#)]
48. Asif, M.; Saeed, M.; Zafar, M.; Amjad, U.-e.-S.; Razzaq, A.; Kim, W.Y. Development of Co–Al LDH/GO composite photocatalyst for enhanced degradation of textile pollutant under visible light irradiation. *Results Phys.* **2022**, *42*, 105997. [[CrossRef](#)]
49. Kaur, H.; Singh, S.; Pal, B. Construction of Ag deposited g-C₃N₄ loaded Co Al LDH ternary composites with aim of pharmaceutical wastewater treatment: Pathways and mechanism for ciprofloxacin degradation. *Appl. Clay Sci.* **2023**, *238*, 106922. [[CrossRef](#)]
50. Chowdhury, P.R.; Medhi, H.; Verma, V.; Kalita, C.; Bhattacharyya, K.G.; Hussain, C.M. Characterisation of Mn/Ti layered double hydroxide for methylene blue degradation with Bayesian representation of electron transport. *Mater. Today Commun.* **2022**, *33*, 104859. [[CrossRef](#)]

51. Dinari, M.; Momeni, M.M.; Ghayeb, Y. Photodegradation of organic dye by ZnCrLa-layered double hydroxide as visible-light photocatalysts. *J. Mater. Sci. Mater. Electron.* **2016**, *27*, 9861–9869. [[CrossRef](#)]
52. Chen, G.; Qian, S.; Tu, X.; Wei, X.; Zou, J.; Leng, L.; Luo, S. Enhancement photocatalytic degradation of rhodamine B on nanoPt intercalated Zn–Ti layered double hydroxides. *Appl. Surf. Sci.* **2014**, *293*, 345–351. [[CrossRef](#)]
53. Wu, L.; Hu, J.; Sun, C.; Jiao, F. Construction of Z-scheme CoAl-LDH/Bi₂MoO₆ heterojunction for enhanced photocatalytic degradation of antibiotics in natural water bodies. *Process Saf. Environ.* **2022**, *168*, 1109–1119. [[CrossRef](#)]
54. Zeng, H.; Zhang, H.; Deng, L.; Shi, Z. Peroxymonosulfate-assisted photocatalytic degradation of sulfadiazine using self-assembled multi-layered CoAl-LDH/g-C₃N₄ heterostructures: Performance, mechanism and eco-toxicity evaluation. *J. Water Process Eng.* **2020**, *33*, 101084. [[CrossRef](#)]
55. Fazli, A.; Brigante, M.; Khataee, A.; Mailhot, G. Synthesis of a magnetically separable LDH-based S-scheme nano-heterojunction for the activation of peroxymonosulfate towards the efficient visible-light photodegradation of diethyl phthalate. *Appl. Surf. Sci.* **2021**, *559*, 149906. [[CrossRef](#)]
56. Abazari, R.; Morsali, A.; Dubal, D.P. An advanced composite with ultrafast photocatalytic performance for the degradation of antibiotics by natural sunlight without oxidizing the source over TMU-5@Ni–Ti LDH: Mechanistic insight and toxicity assessment. *Inorg. Chem. Front.* **2020**, *7*, 2287–2304. [[CrossRef](#)]
57. Huang, X.; Xu, X.; Yang, R.; Fu, X. Synergetic adsorption and photocatalysis performance of g-C₃N₄/Ce-doped MgAl-LDH in degradation of organic dye under LED visible light. *Colloid. Surface A* **2022**, *643*, 128738. [[CrossRef](#)]
58. Khan, A.I.; O’Hare, D. Intercalation chemistry of layered double hydroxides: Recent developments and applications. *J. Mater. Chem.* **2002**, *12*, 3191–3198. [[CrossRef](#)]
59. Weir, M.R.; Moore, J.; Kydd, R.A. Effects of pH and Mg: Ga ratio on the synthesis of gallium-containing layered double hydroxides and their polyoxometalate anion exchanged products. *Chem. Mater.* **1997**, *9*, 1686–1690. [[CrossRef](#)]
60. Busetto, C.; Del Piero, G.; Manara, G.; Trifirò, F.; Vaccari, A. Catalysts for low-temperature methanol synthesis. Preparation of CuZnAl mixed oxides via hydrotalcite-like precursors. *J. Catal.* **1984**, *85*, 260–266. [[CrossRef](#)]
61. Millange, F.; Walton, R.I.; O’Hare, D. Time-resolved in situ X-ray diffraction study of the liquid-phase reconstruction of Mg–Al-carbonate hydrotalcite-like compounds. *J. Mater. Chem.* **2000**, *10*, 1713–1720. [[CrossRef](#)]
62. Zheng, J.; Fan, C.; Li, X.; Yang, Q.; Wang, D.; Duan, A.; Pan, S.; Gao, Y. Simultaneous tailored poly-heptazine units in ZnAl-LDH nanocatalytic surface activation of pollutants and peroxymonosulfate for highly efficient water decontamination. *Chem. Eng. J.* **2024**, *480*, 148234. [[CrossRef](#)]
63. He, S.; Yin, R.; Chen, Y.; Lai, T.; Guo, W.; Zeng, L.; Zhu, M. Consolidated 3D Co₃Mn-layered double hydroxide aerogel for photo-assisted peroxymonosulfate activation in metronidazole degradation. *Chem. Eng. J.* **2021**, *423*, 130172. [[CrossRef](#)]
64. Yekan Motlagh, P.; Khataee, A.; Sadeghi Rad, T.; Hassani, A.; Joo, S.W. Fabrication of ZnFe-layered double hydroxides with graphene oxide for efficient visible light photocatalytic performance. *J. Taiwan Inst. Chem. Eng.* **2019**, *101*, 186–203. [[CrossRef](#)]
65. Ciocarlan, R.G.; Wang, H.; Cuypers, B.; Mertens, M.; Wu, Y.; Van Doorslaer, S.; Seftel, E.M.; Cool, P. ZnTi layered double hydroxides as photocatalysts for salicylic acid degradation under visible light irradiation. *Appl. Clay Sci.* **2020**, *197*, 105757. [[CrossRef](#)]
66. Chen, Q.; Wu, L.; Zhao, X.; Yang, X.-J. Fabrication of Zn–Ti layered double oxide nanosheets with ZnO/ZnTiO₃ heterojunction for enhanced photocatalytic degradation of MO, RhB and MB. *J. Mol. Liq.* **2022**, *353*, 118794. [[CrossRef](#)]
67. Santamaria, L.; Vicente, M.A.; Korili, S.A.; Gil, A. Saline slag waste as an aluminum source for the synthesis of Zn–Al–Fe–Ti layered double-hydroxides as catalysts for the photodegradation of emerging contaminants. *J. Alloys Compd.* **2020**, *843*, 156007. [[CrossRef](#)]
68. Peng, B.; Wu, L.; Li, Q.; Wang, Q.; Li, K.; Zhou, Z. Photodegradation of naproxen using CuZnAl-layered double hydroxides as photocatalysts. *CrystEngComm* **2022**, *24*, 5080–5089. [[CrossRef](#)]
69. Zhou, H.; Zhang, Y. Efficient thermal and photocatalysts made of Au nanoparticles on MgAl-layered double hydroxides for energy and environmental applications. *PCCP* **2019**, *21*, 21798–21805. [[CrossRef](#)]
70. Mkaddem, H.; Rosales, E.; Pazos, M.; Ben Amor, H.; Sanromán, M.A.; Mejjide, J. Anti-inflammatory drug diclofenac removal by a synthesized MgAl layered double hydroxide. *J. Mol. Liq.* **2022**, *359*, 119207. [[CrossRef](#)]
71. Rashidimoghaddam, M.; Saljooqi, A.; Shamspur, T.; Mostafavi, A. Constructing S-doped Ni–Co LDH intercalated with Fe₃O₄ heterostructure photocatalysts for enhanced pesticide degradation. *New J. Chem.* **2020**, *44*, 15584–15592. [[CrossRef](#)]
72. Fang, D.; Huang, L.; Fan, J.; Xiao, H.; Wu, G.; Wang, Y.; Zeng, Z.; Shen, F.; Deng, S.; Ji, F. New insights into the arrangement pattern of layered double hydroxide nanosheets and their ion-exchange behavior with phosphate. *Chem. Eng. J.* **2022**, *441*, 136057. [[CrossRef](#)]
73. Li, L.; Ma, R.; Ebina, Y.; Iyi, N.; Sasaki, T. Positively charged nanosheets derived via total delamination of layered double hydroxides. *Chem. Mater.* **2005**, *17*, 4386–4391. [[CrossRef](#)]
74. Chen, B.Q.; Xia, H.Y.; Mende, L.K.; Lee, C.H.; Wang, S.B.; Chen, A.Z.; Xu, Z.P.; Kankala, R.K. Trends in layered double hydroxides-based advanced nanocomposites: Recent progress and latest advancements. *Adv. Mater. Interfaces* **2022**, *9*, 2200373. [[CrossRef](#)]
75. Taviot-Guého, C.; Prévot, V.; Forano, C.; Renaudin, G.; Mousty, C.; Leroux, F. Tailoring hybrid layered double hydroxides for the development of innovative applications. *Adv. Funct. Mater.* **2017**, *28*, 1703868. [[CrossRef](#)]

76. Venkateshalu, S.; Tomboc, G.M.; Nagalingam, S.P.; Kim, J.; Sawaira, T.; Sehar, K.; Pollet, B.G.; Kim, J.Y.; Nirmala Grace, A.; Lee, K. Synergistic MXene/LDH heterostructures with extensive interfacing as emerging energy conversion and storage materials. *J. Mater. Chem. A* **2023**, *11*, 14469–14488. [CrossRef]
77. Elhalil, A.; Elmoubarki, R.; Sadiq, M.h.; Abdennouri, M.; Kadmi, Y.; Favier, L.; Qourzal, S.; Barka, N. Enhanced photocatalytic degradation of caffeine as a model pharmaceutical pollutant by Ag-ZnO-Al₂O₃ nanocomposite. *Desalin. Water Treat.* **2017**, *94*, 254–262. [CrossRef]
78. Zhang, Z.; Zhao, H.; Ma, X.; Zhang, N.; Meng, Z.; Wang, Y.; Zhao, M.; Liu, H.; Zhang, Q. Construction of MoS₄²⁻ intercalated NiAl-layered double hydroxide by solvent-free method for promoting photocatalytic degradation of antibiotics: Synergistic effect of oxygen vacancies and electron-rich groups. *Sep. Purif. Technol.* **2024**, *337*, 126388. [CrossRef]
79. Liu, Y.; Tang, C.; Cheng, M.; Chen, M.; Chen, S.; Lei, L.; Chen, Y.; Yi, H.; Fu, Y.; Li, L. Polyoxometalate@Metal–Organic framework composites as effective photocatalysts. *ACS Catal.* **2021**, *11*, 13374–13396. [CrossRef]
80. Chang, W.; Qi, B.; Song, Y.-F. Step-by-step assembly of 2D confined chiral space endowing achiral clusters with asymmetric catalytic activity for epoxidation of allylic alcohols. *ACS Appl. Mater. Interfaces* **2020**, *12*, 36389–36397. [CrossRef]
81. Guo, Y.; Li, D.; Hu, C.; Wang, Y.; Wang, E. Layered double hydroxides pillared by tungsten polyoxometalates: Synthesis and photocatalytic activity. *Int. J. Inorg. Mater.* **2001**, *3*, 347–355. [CrossRef]
82. Huang, F.; Tian, S.; Qi, Y.; Li, E.; Zhou, L.; Qiu, Y. Synthesis of FePcS–PMA–LDH cointercalation composite with enhanced visible light photo-Fenton catalytic activity for BPA degradation at circumneutral pH. *Materials* **2020**, *13*, 1951. [CrossRef] [PubMed]
83. Guo, Y.; Li, D.; Hu, C.; Wang, E.; Zou, Y.; Ding, H.; Feng, S. Preparation and photocatalytic behavior of Zn/Al/W(Mn) mixed oxides via polyoxometalates intercalated layered double hydroxides. *Microporous Mesoporous Mater.* **2002**, *56*, 153–162. [CrossRef]
84. Tang, X.; Liu, Y.; Li, S. Heterogeneous UV-Fenton photodegradation of azocarmine B over [FeEDTA]⁻ intercalated ZnAl-LDH at circumneutral pH. *RSC Adv.* **2016**, *6*, 80501–80510. [CrossRef]
85. Wu, J.; Cai, Y.; Zhang, M.; Zhou, J.; Zhou, X.; Shu, W.; Zhang, J.; Huang, X.; Qian, G.; Deng, Y. Enhancing oxidative capability of Ferrate(VI) for oxidative destruction of phenol in water through intercalation of Ferrate(VI) into layered double hydroxide. *Appl. Clay Sci.* **2019**, *171*, 48–56. [CrossRef]
86. Sherryrna, A.; Tahir, M.; Nabgan, W. Recent advancements of layered double hydroxide heterojunction composites with engineering approach towards photocatalytic hydrogen production: A review. *Int. J. Hydrog. Energy* **2022**, *47*, 862–901. [CrossRef]
87. Pelalak, R.; Hassani, A.; Heidari, Z.; Zhou, M. State-of-the-art recent applications of layered double hydroxides (LDHs) material in Fenton-based oxidation processes for water and wastewater treatment. *Chem. Eng. J.* **2023**, *474*, 145511. [CrossRef]
88. Ijaz, M.; Zafar, M. Titanium dioxide nanostructures as efficient photocatalyst: Progress, challenges and perspective. *Int. J. Energ. Res.* **2020**, *45*, 3569–3589. [CrossRef]
89. Ali, I.; Suhail, M.; Alothman, Z.A.; Alwarthan, A. Recent advances in syntheses, properties and applications of TiO₂ nanostructures. *RSC Adv.* **2018**, *8*, 30125–30147. [CrossRef]
90. Suh, M.-J.; Shen, Y.; Chan, C.K.; Kim, J.-H. Titanium dioxide-layered double hydroxide composite material for adsorption-photocatalysis of water pollutants. *Langmuir* **2019**, *35*, 8699–8708. [CrossRef]
91. Grzegórska, A.; Wysocka, I.; Głuchowski, P.; Ryl, J.; Karczewski, J.; Zielińska-Jurek, A. Novel composite of Zn/Ti-layered double hydroxide coupled with MXene for the efficient photocatalytic degradation of pharmaceuticals. *Chemosphere* **2022**, *308*, 136191. [CrossRef]
92. Omrani, E.; Ahmadpour, A.; Heravi, M.; Bastami, T.R. Novel ZnTi LDH/h-BN nanocomposites for removal of two different organic contaminants: Simultaneous visible light photodegradation of Amaranth and Diazepam. *J. Water Process Eng.* **2022**, *47*, 102581. [CrossRef]
93. Liu, Z.; Duan, X.; Sarmah, A.K.; Zhao, X.; Ren, X.; Sun, B. A novel 3-dimensional graphene-based cobalt-manganese bimetallic layered double hydroxide: Formation mechanism and performance in photo-assisted permonosulfate-activated degradation of sulfamethoxazole in aqueous solution. *Environ. Pollut.* **2023**, *336*, 122397. [CrossRef] [PubMed]
94. Yu, Y.; Chen, D.; Xu, W.; Fang, J.; Sun, J.; Liu, Z.; Chen, Y.; Liang, Y.; Fang, Z. Synergistic adsorption-photocatalytic degradation of different antibiotics in seawater by a porous g-C₃N₄/calcined-LDH and its application in synthetic mariculture wastewater. *J. Hazard. Mater.* **2021**, *416*, 126183. [CrossRef] [PubMed]
95. Gholami, P.; Khataee, A.; Soltani, R.D.C.; Dinpazhoh, L.; Bhatnagar, A. Photocatalytic degradation of gemifloxacin antibiotic using Zn-Co-LDH@biochar nanocomposite. *J. Hazard. Mater.* **2020**, *382*, 121070. [CrossRef]
96. Wu, Y.; Wang, H.; Sun, Y.; Xiao, T.; Tu, W.; Yuan, X.; Zeng, G.; Li, S.; Chew, J.W. Photogenerated charge transfer via interfacial internal electric field for significantly improved photocatalysis in direct Z-scheme oxygen-doped carbon nitrogen/CoAl-layered double hydroxide heterojunction. *Appl. Catal. B Environ.* **2018**, *227*, 530–540. [CrossRef]
97. Sun, Y.; Wang, L.; Wang, T.; Liu, X.; Xu, T.; Wei, M.; Yang, L.; Li, C. Improved photocatalytic activity of Ni₂P/NiCo-LDH composites via a Co–P bond charge transfer channel to degrade tetracycline under visible light. *J. Alloys Compd.* **2021**, *852*, 156963. [CrossRef]
98. Zhang, D.; Ji, T.; Yu, J.; Jiang, X.; Jiao, F. Solvothermal synthesis of Cs_{0.33}WO₃/LDHs composite as a novel visible-light-driven photocatalyst. *Photochem. Photobiol.* **2018**, *94*, 219–227. [CrossRef]
99. Zhou, Q.; Jiang, B.; Zhang, L.; Sun, Y.; Yang, X.; Zhang, L. 1D/2D CoNi-LDH/ZnIn₂S₄ S-scheme heterojunction for effectively tetracycline degradation under photocatalytic-peroxymonosulfate activation system: DFT calculations and mechanism insights. *Chem. Eng. J.* **2023**, *478*, 147535. [CrossRef]

100. Ye, C.; Deng, J.; Huai, L.; Cai, A.; Ling, X.; Guo, H.; Wang, Q.; Li, X. Multifunctional capacity of CoMnFe-LDH/LDO activated peroxymonosulfate for p-arsanilic acid removal and inorganic arsenic immobilization: Performance and surface-bound radical mechanism. *Sci. Total Environ.* **2022**, *806*, 150379. [[CrossRef](#)]
101. Hou, X.; Liu, S.; Yu, C.; Jiang, L.; Zhang, Y.; Liu, G.; Zhou, C.; Zhu, T.; Xin, Y.; Yan, Q. A novel magnetic CuFeAl-LDO catalyst for efficient degradation of tetrabromobisphenol A in water. *Chem. Eng. J.* **2022**, *430*, 133107. [[CrossRef](#)]
102. Chen, M.; Li, S.; Li, L.; Jiang, L.; Ahmed, Z.; Dang, Z.; Wu, P. Memory effect induced the enhancement of uranium (VI) immobilization on low-cost MgAl-double oxide: Mechanism insight and resources recovery. *J. Hazard. Mater.* **2021**, *401*, 123447. [[CrossRef](#)] [[PubMed](#)]
103. Shen, J.-C.; Zeng, H.-Y.; Chen, C.-R.; Xu, S. A facile fabrication of Ag₂O-Ag/ZnAl-oxides with enhanced visible-light photocatalytic performance for tetracycline degradation. *Appl. Clay Sci.* **2020**, *185*, 105413. [[CrossRef](#)]
104. Feng, X.; Yu, Z.; Shan, M.; Long, R.; Li, X.; Liao, K. Z-type ZnAl-LDO/Ag₂S heterojunction activated peroxy sulfate to degrade tetracycline hydrochloride under visible light efficiently. *Chem. Eng. J.* **2022**, *443*, 136422. [[CrossRef](#)]
105. Elhalil, A.; Elmoubarki, R.; Machrouhi, A.; Sadiq, M.; Abdennouri, M.; Qourzal, S.; Barka, N. Photocatalytic degradation of caffeine by ZnO-ZnAl₂O₄ nanoparticles derived from LDH structure. *J. Environ. Chem. Eng.* **2017**, *5*, 3719–3726. [[CrossRef](#)]
106. Zheng, X.; Dong, Y.; Zhu, Q. Enhanced photocatalysis of MgAl layered double oxide nanosheets with B, N-codoped carbon coating for tetracycline removal. *Appl. Clay Sci.* **2020**, *193*, 105694. [[CrossRef](#)]
107. Zhang, J.; Gao, M.; Wang, R.; Li, X.; Wang, J.; Li, S.; Cao, K.; Li, J.; Wang, Y.; Zheng, Z. Bifunctional role of oxygen vacancy in LDH supported Au nanoparticles catalyst for selective photocatalytic hydrogenation of cinnamaldehyde. *Fuel* **2024**, *365*, 131235. [[CrossRef](#)]
108. Azalok, K.A.; Oladipo, A.A.; Gazi, M. Hybrid MnFe-LDO–biochar nanopowders for degradation of metronidazole via UV-light-driven photocatalysis: Characterization and mechanism studies. *Chemosphere* **2021**, *268*, 128844. [[CrossRef](#)] [[PubMed](#)]
109. Azalok, K.A.; Oladipo, A.A.; Gazi, M. UV-light-induced photocatalytic performance of reusable MnFe-LDO–biochar for tetracycline removal in water. *J. Photoch. Photobio. A* **2021**, *405*, 112976. [[CrossRef](#)]
110. Gao, K.; Huang, D.; Hou, L.-a.; An, X.; Takizawa, S.; Yang, Y. Efficient degradation of carbamazepine by sulfate doped LDO/CN in the photo-assisted peroxy monosulfate system. *Chem. Eng. J.* **2024**, *482*, 149034. [[CrossRef](#)]
111. Di, G.; Zhu, Z.; Zhang, H.; Zhu, J.; Lu, H.; Zhang, W.; Qiu, Y.; Zhu, L.; Küppers, S. Simultaneous removal of several pharmaceuticals and arsenic on Zn-Fe mixed metal oxides: Combination of photocatalysis and adsorption. *Chem. Eng. J.* **2017**, *328*, 141–151. [[CrossRef](#)]
112. Elhalil, A.; Elmoubarki, R.; Farnane, M.; Machrouhi, A.; Mahjoubi, F.Z.; Sadiq, M.; Qourzal, S.; Barka, N. Synthesis, characterization and efficient photocatalytic activity of novel Ca/ZnO-Al₂O₃ nanomaterial. *Mater. Today Commun.* **2018**, *16*, 194–203. [[CrossRef](#)]
113. Wang, M.; Wang, J.; Li, M.; Wang, X.; Sima, Y.; Wu, Q. Novel In₂S₃/Zn–Al LDHs composite as an efficient visible-light-driven photocatalyst for tetracycline degradation. *Opt. Mater.* **2022**, *128*, 112376. [[CrossRef](#)]
114. Li, X.; Ma, T.; Dong, L.; Na, Y.; Liu, Y.; Li, Z.; Zheng, R.; Dai, S.; Zhao, T. Mechanochemical homodisperse of Bi₂MoO₆ on Zn-Al LDH matrix to form Z-scheme heterojunction with promoted visible-light photocatalytic performance. *Adv. Powder Technol.* **2022**, *33*, 103468. [[CrossRef](#)]
115. Zhang, H.; Nengzi, L.-c.; Wang, Z.; Zhang, X.; Li, B.; Cheng, X. Construction of Bi₂O₃/CuNiFe LDHs composite and its enhanced photocatalytic degradation of lomefloxacin with persulfate under simulated sunlight. *J. Hazard. Mater.* **2020**, *383*, 121236. [[CrossRef](#)] [[PubMed](#)]
116. Li, Q.; Wei, G.; Duan, G.; Zhang, L.; Li, Z.; Wei, Z.; Zhou, Q.; Pei, R. Photocatalysis activation of peroxydisulfate over oxygen vacancies-rich mixed metal oxide derived from red mud-based layered double hydroxide for ciprofloxacin degradation. *Sep. Purif. Technol.* **2022**, *289*, 120733. [[CrossRef](#)]
117. Sun, C.; Wang, Y.; Wu, L.; Hu, J.; Long, X.; Wu, H.; Jiao, F. In situ preparation of novel p–n junction photocatalyst MgAl-LDH/(BiO)₂CO₃ for enhanced photocatalytic degradation of tetracycline. *Mater. Sci. Semicond. Process.* **2022**, *150*, 106939. [[CrossRef](#)]
118. Sadeghi Rad, T.; Khataee, A.; Arefi-Oskoui, S.; Sadeghi Rad, S.; Orooji, Y.; Gengec, E.; Kobya, M. Graphene-based ZnCr layered double hydroxide nanocomposites as bactericidal agents with high sonophotocatalytic performances for degradation of rifampicin. *Chemosphere* **2022**, *286*, 131740. [[CrossRef](#)]
119. Shen, J.; Shi, A.; Lu, J.; Lu, X.; Zhang, H.; Jiang, Z. Optimized fabrication of Cu-doped ZnO/calcined CoFe–LDH composite for efficient degradation of bisphenol A through synergistic visible-light photocatalysis and persulfate activation: Performance and mechanisms. *Environ. Pollut.* **2023**, *323*, 121186. [[CrossRef](#)] [[PubMed](#)]
120. Sadeghi Rad, T.; Khataee, A.; Sadeghi Rad, S.; Arefi-Oskoui, S.; Gengec, E.; Kobya, M.; Yoon, Y. Zinc-chromium layered double hydroxides anchored on carbon nanotube and biochar for ultrasound-assisted photocatalysis of rifampicin. *Ultrason. Sonochem.* **2022**, *82*, 105875. [[CrossRef](#)]
121. Sheikhpour, H.; Saljooqi, A.; Shamspur, T.; Mostafavi, A. Co-Al Layered double hydroxides decorated with CoFe₂O₄ nanoparticles and g-C₃N₄ nanosheets for efficient photocatalytic pesticide degradation. *Environ. Technol. Innov.* **2021**, *23*, 101649. [[CrossRef](#)]
122. Zheng, J.; Tang, X.; Fan, C.; Deng, Y.; Li, X.; Yang, Q.; Wang, D.; Duan, A.; Luo, J.; Chen, Z.; et al. Facile synthesis of Ag@AgCl/ZnAl-LDH sesame balls nanocomposites with enhanced photocatalytic performance for the degradation of neonicotinoid pesticides. *Chem. Eng. J.* **2022**, *446*, 136485. [[CrossRef](#)]

123. Zheng, J.; Li, W.; Tang, R.; Xiong, S.; Gong, D.; Deng, Y.; Zhou, Z.; Li, L.; Su, L.; Yang, L. Ultrafast photodegradation of nitenpyram by Ag/Ag₃PO₄/Zn–Al LDH composites activated by persulfate system: Removal efficiency, degradation pathway and reaction mechanism. *Chemosphere* **2022**, *292*, 133431. [[CrossRef](#)] [[PubMed](#)]
124. Zheng, J.; Deng, Y.; Fan, C.; Li, X.; Gong, D.; Li, C.; Ye, Z. Novel Zn–Al LDHs based S-scheme heterojunction with coral reef-like structure for photocatalytic activation of peroxydisulfate towards nitenpyram decomposition. *J. Environ. Chem. Eng.* **2022**, *10*, 108188. [[CrossRef](#)]
125. Zheng, J.; Fan, C.; Li, X.; Yang, Q.; Wang, D.; Duan, A.; Pan, S. Efficient mineralisation and disinfection of neonicotinoid pesticides with unique ZnAl-LDH intercalation structure and synergistic effect of Cu₂O crystalline surface. *Colloid. Surface. A* **2024**, *687*, 133507. [[CrossRef](#)]
126. Li, E.; Liao, L.; Lv, G.; Li, Z.; Yang, C.; Lu, Y. The Interactions Between Three Typical PPCPs and LDH. *Front. Chem.* **2018**, *6*, 00016. [[CrossRef](#)] [[PubMed](#)]
127. Gao, Z.; Liang, J.; Yao, J.; Meng, Q.; He, G.; Chen, H. Synthesis of Ce-doped NiAl LDH/RGO composite as an efficient photocatalyst for photocatalytic degradation of ciprofloxacin. *J. Environ. Chem. Eng.* **2021**, *9*, 105405. [[CrossRef](#)]
128. Mourid, E.H.; El Mouchtari, E.M.; El Mersly, L.; Benaziz, L.; Rafqah, S.; Lakraimi, M. Development of a new recyclable nanocomposite LDH-TiO₂ for the degradation of antibiotic sulfamethoxazole under UVA radiation: An approach towards sunlight. *J. Photochem. Photobiol. A* **2020**, *396*, 112530. [[CrossRef](#)]
129. Arjomandi-Behzad, L.; Alinejad, Z.; Zandragh, M.R.; Golmohamadi, A.; Vojoudi, H. Facile synthesis of hollow spherical g-C₃N₄@LDH/NCQDs ternary nanostructure for multifunctional antibacterial and photodegradation activities. *iScience* **2023**, *26*, 106213. [[CrossRef](#)]
130. Xiong, J.; Zeng, H.-Y.; Peng, J.-F.; Wang, L.-H.; Peng, D.-Y.; Liu, F.-Y.; Xu, S.; Yang, Z.-L. Fabrication of Cu₂O/ZnTi-LDH p-n heterostructure by grafting Cu₂O NPs onto the LDH host layers from Cu-doped ZnTi-LDH and insight into the photocatalytic mechanism. *Compos. Part B Eng.* **2023**, *250*, 110447. [[CrossRef](#)]
131. Rodgers, K.M.; Swartz, C.H.; Occhialini, J.; Bassignani, P.; McCurdy, M.; Schaidler, L.A. How Well Do Product Labels Indicate the Presence of PFAS in Consumer Items Used by Children and Adolescents? *Environ. Sci. Technol.* **2022**, *56*, 6294–6304. [[CrossRef](#)]
132. Schulz, K.; Silva, M.R.; Klaper, R. Distribution and effects of branched versus linear isomers of PFOA, PFOS, and PFHxS: A review of recent literature. *Sci. Total Environ.* **2020**, *733*, 139186. [[CrossRef](#)] [[PubMed](#)]
133. Michaels, R.A. Lessons learned from legacy contaminants of emerging concern: Perfluoroalkyl compounds (PFCs) in the village of Hoosick Falls, Rensselaer County, New York. *Environ. Claims J.* **2017**, *29*, 4–48. [[CrossRef](#)]
134. Tang, H.; Zhang, W.; Meng, Y.; Xia, S. A direct Z-scheme heterojunction with boosted transportation of photogenerated charge carriers for highly efficient photodegradation of PFOA: Reaction kinetics and mechanism. *Appl. Catal. B Environ.* **2021**, *285*, 119851. [[CrossRef](#)]
135. Yang, Y.; Ji, W.; Li, X.; Zheng, Z.; Bi, F.; Yang, M.; Xu, J.; Zhang, X. Insights into the degradation mechanism of perfluorooctanoic acid under visible-light irradiation through fabricating flower-shaped Bi₅O₇I/ZnO n-n heterojunction microspheres. *Chem. Eng. J.* **2021**, *420*, 129934. [[CrossRef](#)]
136. Yang, H.; Park, S.-J.; Lee, C.-G. Enhanced removal of perfluoroalkyl substances using MMO-TiO₂ visible light photocatalyst. *Alex. Eng. J.* **2024**, *87*, 31–38. [[CrossRef](#)]
137. Sohrabi, H.; Arbabzadeh, O.; Falaki, M.; Majidi, M.R.; Han, N.; Yoon, Y.; Khataee, A. Electrochemical layered double hydroxide (LDH)-based biosensors for pesticides detection in food and environment samples: A review of status and prospects. *Food Chem. Toxicol.* **2022**, *164*, 113010. [[CrossRef](#)] [[PubMed](#)]
138. Tian, X.; Hong, X.; Yan, S.; Li, X.; Wu, H.; Lin, A.; Yang, W. Neonicotinoids caused oxidative stress and DNA damage in juvenile Chinese rare minnows (*Gobiocypris rarus*). *Ecotox. Environ. Saf.* **2020**, *197*, 110566. [[CrossRef](#)] [[PubMed](#)]
139. Azizi, D.; Arif, A.; Blair, D.; Dionne, J.; Fillion, Y.; Ouarda, Y.; Pazmino, A.G.; Pulicharla, R.; Rilstone, V.; Tiwari, B.; et al. A comprehensive review on current technologies for removal of endocrine disrupting chemicals from wastewaters. *Environ. Res.* **2022**, *207*, 112196. [[CrossRef](#)]
140. Xu, Q.; Huang, Q.-S.; Luo, T.-Y.; Wu, R.-L.; Wei, W.; Ni, B.-J. Coagulation removal and photocatalytic degradation of microplastics in urban waters. *Chem. Eng. J.* **2021**, *416*, 129123. [[CrossRef](#)]
141. Arjomandi-Behzad, L.; Zandragh, M.R.; Alinejad, Z.; Golmohamadi, A.; Vojoudi, H. Hollow core-shell LDH@N-HCS/CN S-scheme photocatalyst with the enhanced visible-light activity. *J. Environ. Chem. Eng.* **2023**, *11*, 109574. [[CrossRef](#)]
142. He, Y.; Rehman, A.U.; Xu, M.; Not, C.A.; Ng, A.M.C.; Djurišić, A.B. Photocatalytic degradation of different types of microplastics by TiO_x/ZnO tetrapod photocatalysts. *Heliyon* **2023**, *9*, e22562. [[CrossRef](#)] [[PubMed](#)]
143. Rodrigues, M.O.; Abrantes, N.; Gonçalves, F.J.M.; Nogueira, H.; Marques, J.C.; Gonçalves, A.M.M. Spatial and temporal distribution of microplastics in water and sediments of a freshwater system (Antuã River, Portugal). *Sci. Total Environ.* **2018**, *633*, 1549–1559. [[CrossRef](#)] [[PubMed](#)]
144. Jiang, S.; Yin, M.; Ren, H.; Qin, Y.; Wang, W.; Wang, Q.; Li, X. Novel CuMgAlTi-LDH photocatalyst for efficient degradation of microplastics under visible light irradiation. *Polymers* **2023**, *15*, 2347. [[CrossRef](#)] [[PubMed](#)]

Disclaimer/Publisher’s Note: The statements, opinions and data contained in all publications are solely those of the individual author(s) and contributor(s) and not of MDPI and/or the editor(s). MDPI and/or the editor(s) disclaim responsibility for any injury to people or property resulting from any ideas, methods, instructions or products referred to in the content.